

CONFIDENTIAL

Copy 5
RM 151104

DEC 4 1951

FOR REFERENCE

NACA

NOT TO BE TAKEN FROM THIS ROOM

RESEARCH MEMORANDUM

FLIGHT DETERMINATION OF THE DRAG AND LONGITUDINAL STABILITY
AND CONTROL CHARACTERISTICS OF A ROCKET-POWERED
MODEL OF A 60° DELTA-WING AIRPLANE FROM

MACH NUMBERS OF 0.75 TO 1.70

By Grady L. Mitcham, Norman L. Crabill,
and Joseph E. Stevens

Langley Aeronautical Laboratory
Langley Field, Va.

CLASSIFICATION CHANGED

UNCLASSIFIED

CLASSIFIED DOCUMENT

This material contains information affecting the National Defense of the United States within the meaning of the espionage laws, Title 18, U.S.C., Secs. 793 and 794, the transmission or revelation of which in any manner to unauthorized person is prohibited by law.

NATIONAL ADVISORY COMMITTEE
FOR AERONAUTICS

WASHINGTON
November 29, 1951

NACA LIBRARY

CONFIDENTIAL

LANGLEY AERONAUTICAL LABORATORY
Langley Field, Va.

Classified
By authority of 48 CFR 1.126
Date 10-13-57
NB 10-9-57



3 1176 01436 4534

NATIONAL ADVISORY COMMITTEE FOR AERONAUTICS

RESEARCH MEMORANDUM

FLIGHT DETERMINATION OF THE DRAG AND LONGITUDINAL STABILITY
AND CONTROL CHARACTERISTICS OF A ROCKET-POWERED
MODEL OF A 60° DELTA-WING AIRPLANE FROM

MACH NUMBERS OF 0.75 TO 1.70

By Grady L. Mitcham, Norman L. Crabill,
and Joseph E. Stevens

SUMMARY

A flight investigation has been conducted to determine the aerodynamic characteristics of a model of a tailless delta-wing-airplane configuration having a leading edge swept back 60° . These data for the Mach number range between 0.75 and 1.70 were obtained by analyzing the model responses to abrupt up and down elevon control movements.


The variation of lift-curve slope C_{L_α} with Mach number was gradual. Buffeting occurred as maximum lift coefficient was approached at high subsonic speeds although no buffet was present at the lower lift coefficients.

The drag rise began at approximately $M = 0.90$; the greatest minimum drag coefficient was about 0.04 at $M = 1.15$. The variation of drag with lift, with the elevon neutral, indicated that the resultant force vector was inclined forward of the normal to the wing at all Mach numbers of the test.

There was a large increase in hinge-moment coefficients at supersonic speeds. The elevon was an effective control throughout the speed range covered, although the effectiveness was reduced at supersonic speeds.

The transonic trim change was mild.

The model was both statically and dynamically stable with the center of gravity located at 20.7 percent mean aerodynamic chord. The aerodynamic-center location shifted 11 percent of the mean aerodynamic chord throughout the Mach number range.



INTRODUCTION

Triangular-wing plan forms with various degrees of sweepback and thickness ratios have been proposed for aircraft designed to fly at transonic and supersonic speeds. As a result of one of these proposals, the NACA has conducted a flight investigation with rocket-powered models to determine lift, drag, and longitudinal stability and control characteristics at transonic and supersonic speeds of a delta-wing tailless airplane configuration.

The results of the longitudinal stability and control investigation obtained from the flight tests of three models of the same configuration at Mach numbers of 0.75 to 1.28 have been presented in reference 1. The primary purpose of the test reported herein was to obtain the variation of drag with lift in the Mach number range from 0.75 to 1.70. In addition to the drag results, stability derivatives and other aerodynamic parameters evaluated from the flight are presented.

SYMBOLS

a	acceleration, feet per second ²
A	wing aspect ratio (b^2/S)
b	wing span, feet
b _e	elevon span at trailing edge, feet
\bar{c}	wing mean aerodynamic chord, feet
\bar{c}_e	mean chord of elevon area aft of hinge axis, feet
C _c	chord-force coefficient, positive in a forward direction $\left(\frac{a_l}{g} \frac{W}{S} \frac{1}{q}\right)$
C _D	drag coefficient $(C_N \sin \alpha - C_c \cos \alpha)$
C _{D_b}	base drag coefficient $\left(\frac{\Delta p}{q} \frac{\text{Area base}}{S}\right)$
C _{D_{min}}	minimum drag coefficient

C_h	hinge-moment coefficient $\left(\frac{\text{Hinge moment}}{qb_e \bar{c}_e^2} \right)$
C_{h_0}	hinge-moment coefficient at zero angle of attack and elevon deflection
C_L	lift coefficient $(C_N \cos \alpha + C_c \sin \alpha)$
C_{L_0}	lift coefficient at minimum drag
C_m	pitching-moment coefficient $\left(\frac{\text{Pitching moments about center of gravity}}{qS\bar{c}} \right)$
C_{m_0}	pitching-moment coefficient at zero angle of attack and elevon deflection
C_N	normal-force coefficient, positive toward top of model from model center line $\left(\frac{a_n}{g} \frac{W}{S} \frac{1}{q} \right)$
g	acceleration due to gravity (32.2 ft/sec ²)
I_y	moment of inertia about pitch axis
$\left(\frac{L}{D} \right)_{\max}$	maximum lift-drag ratio
M	Mach number
p	free-stream static pressure, pounds per square foot
P	period, seconds
q	dynamic pressure, pounds per square foot $\left(\frac{\gamma p}{2} M^2 \right)$
R	Reynolds number based on wing mean aerodynamic chord
S	wing area including body intercept
t	time, seconds
$T_{1/2}$	time to damp to one-half amplitude, seconds

V	velocity, feet per second
W	weight of model, pounds
α	angle of attack at model center of gravity, degrees
γ	specific heat ratio (1.4)
δ	elevon deflection, positive, trailing edge down, degrees
Δ	increment
θ	angle between fuselage center line and horizontal
$\omega = \frac{2\pi}{P}$	

Derivatives:

$$C_{L_\alpha} = \frac{\partial C_L}{\partial \alpha}, \quad C_{h_\delta} = \frac{\partial C_h}{\partial \delta}, \text{ and so forth}$$

$$\dot{\theta} = \frac{d\theta}{dt}, \text{ and so forth, radians per second}$$

Subscripts:

ind	indicated
l	longitudinal
n	normal
trim	denotes trim condition

MODELS AND APPARATUS

Models

A three-view drawing of the model used in the flight investigation is given in figure 1 and the physical characteristics of the model are presented in table I. Photographs of the model are presented as figures 2 and 3. The model fuselage and components were constructed of duralumin, magnesium castings, and magnesium skin. The model had a

delta wing with 60° sweepback of the leading edge and an aspect ratio of 2.31, the profile at all spanwise stations being an NACA 65(06)A006.5 section. Longitudinal control was provided by a single set of constant-chord control surfaces (elevons) on the wing trailing edge. Deflecting the elevons together provided longitudinal control and, in a full-scale airplane, deflecting them differentially would give lateral control. The vertical fin of the model was of triangular plan form with a leading-edge sweepback of 60° and had the same airfoil section as the wing.

Prior to the flight, a known static load was applied at a point about midspan of the elevon and the deflections at the root and midspan were measured; this calibration in conjunction with the recorded hinge-moment data was used to correct the control positions recorded during the flight test to an average spanwise value.

The movement of the elevons called for abrupt pull-ups and push-downs operating at a frequency of about one cycle per second. The unsealed control surfaces were pulsed between about neutral ($\delta = 0^\circ$) and -9° in an approximate square-wave motion throughout the coasting phase of the flight.

The wing loading of the model was 30.94 pounds per square foot, and the center of gravity was at 20.7 percent of the mean aerodynamic chord.

Prior to flight testing, the model was suspended by shock cords and shaken with an electromagnetic shaker at frequencies up to 400 cycles per second. A fundamental frequency of 103 cycles per second was observed from the telemeter record taken during the ground tests. Only the normal acceleration channel showed any frequency response in the ground tests. Resonances occurred at 103, 162, 198, and 222 cycles per second.

The technique of launching and boosting the model to supersonic speeds was essentially the same as the technique described in reference 1. A photograph of the booster-model combination prior to launching is shown as figure 4.

Apparatus

The flight time history as the model traversed the speed range was transmitted and recorded by a telemeter system which gave eight channels of information. The measurements made were normal and longitudinal acceleration, control position, hinge moment, angle of attack, total pressure, base pressure on the rear of the model, and a reference static pressure for determining Mach number and dynamic pressure. Instrumentation arrangement in a typical model is shown in figure 5. The angle

of attack was measured by a vane-type indicator located on a sting ahead of the nose of the model. A description of this indicator can be found in reference 2. Due to instrument limitations, the range of angles of attack that can be measured is approximately $\pm 15^\circ$ relative to the center line of the indicator. In the test reported herein the sting was deflected down 10° from the center line of the model (fig. 1) in order to record higher positive values of angle of attack. A radiosonde released at firing was used to obtain free-stream temperature and static pressure. Ground equipment consisting of a CW Doppler radar unit and a radar tracking unit was used to determine model velocity and position in space.

ANALYSIS OF DATA

All the data discussed herein were obtained during the decelerating portion of the flight. The methods of analysis used in reducing the data from the flight time history apply to the free oscillation resulting from a step function disturbance. This disturbance was created by pulsing the elevons up and down in an approximate square-wave motion which resulted in changes in normal acceleration, angle of attack, and hinge moment. The longitudinal stability was indicated by the period and rate of decay of the short-period longitudinal oscillations during the period when the controls were held fixed between pulses. The analysis of these longitudinal oscillations is based on two degrees of freedom, acceleration normal to the flight path and rotation in pitch about the center of gravity. A more complete discussion of the methods and corrections used in reducing these data from the flight time-history records to the parameters presented in this paper is given in the appendixes of references 1 and 3.

Since the primary purpose of this test was the determination of the effect of lift on drag, it was necessary to determine, as accurately as possible, the minimum drag with neutral elevon. Therefore, to allow any flow separation effects induced by the high angle-of-attack portion of the cycle an opportunity to disappear, the data presented for neutral elevon are taken from the second peak following the control movement, except at a Mach number of 0.74, where only one peak was obtained due to the decreased stability of the model. At this Mach number the data are from the first peak. The angle of attack at the indicator was corrected to the center-of-gravity location as in reference 1 and plotted as a function of time. The corrected angles of attack were then used in conjunction with the values of normal-force coefficient C_N and chord-force coefficient C_C to compute lift coefficient C_L and drag coefficient C_D .

The high angles of attack in combination with the high values of $C_{h\alpha}$ of the unbalanced elevon resulted in variations in δ on the order of 1.5° during the oscillations. Therefore, the lift coefficient was corrected by the equation

$$C_L = C_{L_{ind}} - C_{L_\delta} \Delta\delta$$

following the method of reference 1. By this method the lift data obtained at approximately zero deflection were corrected to zero ($\Delta\delta = \delta$) and that obtained at about -9° corrected to -9° ($\Delta\delta = \delta + 9^\circ$).

No corrections, due to elevon system flexibility, were applied to the drag, as it was estimated that over the range of $\Delta\delta$'s encountered, the ΔC_D values would be within the limits of accuracy of the drag data.

The functions $C_{D_{min}}$, C_{L_0} , and dC_D/dC_L^2 were determined by plotting C_D against C_L and C_D against $(C_L - C_{L_0})^2$ and fairing curves of the form

$$C_D = C_{D_{min}} + \frac{dC_D}{dC_L^2} (C_L - C_{L_0})^2$$

through the data points. The curve so faired generally fell between the data points obtained with increasing angle of attack and those obtained with decreasing angle of attack within the probable accuracy of the test.

ACCURACY

The limitations of the technique employed are discussed thoroughly in reference 4. In order to adapt the discussion presented therein to the present paper, it is only necessary to reestimate the maximum possible errors in the absolute value of C_L and C_D , due to the different normal and longitudinal accelerometer ranges. It should be emphasized

that the probable error due to this source is much less than the values presented in the following table:

M	ΔC_L	ΔC_D
0.90	± 0.03	± 0.009
1.50	± 0.01	± 0.002

RESULTS AND DISCUSSION

The Reynolds number range for this test is given as a function of Mach number in figure 6.

Lift

Lift-curve slope.- Typical curves of lift coefficient plotted against angle of attack are shown for Mach numbers of 1.56, 1.32, 0.82, and 0.77 in figure 7. Different symbols are used for ascending and descending values of angle of attack. At $M = 1.56$, there is very little phase difference between the ascending and descending values of angle of attack. There is, however, a phase lag of angle of attack with lift coefficient at $M = 0.82$. An investigation of the instrument responses did not reveal it possible to obtain any phase lag of comparable magnitude to those encountered in this test. The lift derivatives C_{L_α} and C_{L_θ} contributed only about 18 percent of the maximum lag at $M = 0.82$. This phase-lag effect has been evident in data obtained from other pulsed control models. One of the contributing factors to this effect could possibly be the result of asymmetric air-flow separation. This is substantiated by the increased phase lag at the lift coefficients where flow separation has probably occurred as shown in figure 7.

The variation of lift-curve slope C_{L_α} with Mach number is shown in figure 8. These values of lift-curve slope are average slopes taken for $C_L < 0.25$ elevon neutral and $0.25 < C_L < 0.50$ elevon deflected -9° , since some nonlinearity was evident for lift coefficient plotted against angle of attack. The results of previous tests (reference 1) shown in figure 8 did not show this nonlinearity; however, this was probably due to the limited amount of data obtained at the higher lift coefficients. Theoretical values of C_{L_α} for a delta wing obtained from reference 5 have been corrected for the effect of the fuselage by the method of

reference 6 and plotted for comparison in figure 8. The results of the present test show a gradual variation of $C_{L\alpha}$ with Mach number from $M = 0.75$ to $M = 1.70$ with a maximum value of $C_{L\alpha}$ of 0.054 near $M = 1.0$.

Lift summary.- A summary of the lift data which includes the buffet boundary and the maximum C_L attained in the test as functions of Mach number is presented in figure 9. At $M = 0.77$ and $M = 0.82$ (compare fig. 7), the model apparently was operating near maximum lift coefficient; however, this could not be definitely ascertained since the angle-of-attack vane was against its limit stop. The nonlinearity of C_L with α near maximum lift coefficient can also be seen in figures 7 and 9.

Buffet.- Examination of the flight time history showed the presence of high frequency oscillations in the normal acceleration trace at the higher lift coefficients below $M = 0.94$. These oscillations probably were the result of unsteady separated air flow developed during the test at the higher lift coefficients. A section of the flight time history showing the existence of this buffet phenomenon is presented in figure 10. Buffeting boundary, as discussed in this paper, refers to the lift coefficient at which buffeting starts as indicated by the appearance of the high frequency oscillation in the normal acceleration trace. Inspection of figure 10 shows that the model did not buffet at the lower lift coefficients. It can be seen, however, that where buffeting occurred, the oscillation continues to a lift coefficient lower than the point of origin. This may be attributed to some aerodynamic effect or may represent low structural damping of the wing, as the same effect was evidenced in the tests reported in references 7 and 8 where buffeting was encountered. It should be pointed out that the amplitudes of the buffeting oscillations are larger by a factor of approximately 1.5 than indicated by the flight records, because of the reduced amplitude response characteristics of the telemetering system at the frequencies encountered in this test (108 to 113 cycles per second). It may be noted that these oscillations occur near the frequency of the first bending mode of the wing (103 cycles per second). This same trend was evidenced in references 7 to 9. High frequency oscillations were also encountered in the flight test of a previous model of the same configuration with a more flexible wing; an analysis of these oscillations (reference 10) proved them to be flutter. These oscillations encountered in reference 10 occurred at lift coefficients near zero and the ratio of the frequency of oscillation to the natural torsional frequency was about 0.74 which compared favorably with ratios of flutter frequency to torsional frequency which were obtained in the Langley 4.5-foot flutter research tunnel for a 45° delta wing (unpublished data). Therefore, the oscillations recorded in the test reported herein at the high lift coefficients and at the frequency of the first bending mode are believed

to be the result of the buffet phenomenon, not flutter. In figure 9 the buffeting boundary is presented in terms of lift coefficient as a function of Mach number. These data (particularly the buffet amplitudes) may not be directly applicable to a full-scale airplane because of the instrumentation limitations as previously stated and the difference in the mass and stiffness characteristics of the model and airplane.

Drag

Minimum drag.- The variation of the minimum drag coefficient $C_{D_{min}}$ and the lift coefficient for minimum drag C_{L_0} are presented as functions of Mach number in figures 11 and 12, respectively. Base drag coefficients are included in all the drag coefficients.

In the neutral elevon condition, the drag rise occurs at about $M = 0.90$. The greatest value of the minimum drag coefficient is about 0.040 and occurs at about $M = 1.15$.

The lift coefficient at minimum drag exhibits its maximum value, about 0.05, at about the same Mach number and decreases to a minimum of about 0.02 at $M = 0.94$ and to 0.030 at $M = 1.6$.

Deflecting the elevon up 9° produces an increase in the minimum drag coefficient on the order of 0.005 at $M = 1.6$, but does not alter the general shape of the curve. The drag rise still occurs at $M = 0.90$, and the greatest value occurs at $M = 1.13$. Conversely, the magnitude of the lift coefficient at minimum drag is decreased, although the same general variation with Mach number is still obtained.

Base drag.- The base pressure of the model was measured at one point and a flat pressure distribution was assumed (angle-of-attack range was between $\pm 1^\circ$). The base pressure drag coefficient, based on model wing area, is given as a function of Mach number in figure 11. No data are presented below $M = 0.90$ because of large possible errors in this portion of the speed range, due to the high rates of change in angle of attack.

Variation of drag with lift.- The drag coefficients for several lift coefficients up to the maximum obtained are presented in figures 13 and 14 as functions of Mach number for the neutral and -9° elevon deflection, respectively. The data obtained at $M = 0.74$ are from the first peak after the control returns to neutral, and may therefore not be directly comparable to the data obtained at higher Mach numbers.

The variation of C_D with $(C_L - C_{L_0})^2$, dC_D/dC_L^2 , has been determined, and is presented as a function of Mach number in figure 15(a) for neutral elevon. Comparison of dC_D/dC_L^2 , elevon neutral, with $1/C_{L_\alpha}$ shows that at all Mach numbers, the resultant-force vector is rotated forward of the perpendicular to the wing. At subsonic Mach numbers, dC_D/dC_L^2 is greater than $1/\pi A$. At the lowest subsonic speeds of the test, there is evidence of some nonlinearity in dC_D/dC_L^2 , which tends to increase markedly above a C_L of about 0.22.

A comparison between the experimental results obtained in the present test for the wing-fuselage combination with theoretical results for a wing alone (obtained from the analysis of reference 11) shows that in the present test, with neutral elevon, the resultant-force vector is tilted forward of the normal to the wing from 50 percent at $M = 1.0$ to 30 percent at $M = 1.7$ of the amount predicted by theory for the wing alone.

Deflecting the elevon up 9° results in greater drag at all lift coefficients. Comparison of the drag parameter dC_D/dC_L^2 with $1/C_{L_\alpha}$, figure 15(b), shows that, at all supersonic speeds, the resultant-force vector is inclined rearward from the perpendicular to the plane of the airfoil. At subsonic speeds, however, the resultant-force vector is apparently tilted forward slightly. The lift coefficient corresponding to the break in the variation of C_D with $(C_L - C_{L_0})^2$ has also been increased from 0.22 to 0.32 at subsonic Mach numbers.

Lift-drag ratio.— The maximum lift-drag ratios $(L/D)_{\max}$ and the lift coefficient for $(L/D)_{\max}$ are plotted as functions of Mach number in figure 16 for neutral and -9° elevon deflections. No data appear above $M = 0.90$, with neutral elevon, since the maximum C_L attained is less than the C_L for $(L/D)_{\max}$ in this Mach number range. The maximum lift-drag ratios presented vary from 7.6 to about 9. Plots of the variation of L/D with C_L are also presented for several representative Mach numbers in figure 17.

The lift-drag ratios with elevon deflected are seen to be from three-fourths to one-half those obtained with the elevon neutral. The maximum lift coefficient attained falls below the lift coefficient for $(L/D)_{\max}$ above $M = 1.21$, precluding the determination of it and $(L/D)_{\max}$ above that Mach number. The low value of $(L/D)_{\max}$ at $M = 0.77$ is due to the scatter in the minimum drag at this Mach number.

Effect of elevon deflection on drag. - Since the elevon comprises such a large percentage of the wing and has a correspondingly large effect on drag it is desirable to be able to compute the drag at various trim elevon deflections and lift coefficients. The general equation for drag as a function of lift due to angle of attack is of the form:

$$C_D = C_{D_{min}} + \frac{dC_D}{dC_L^2} (C_L - C_{L_0})^2$$

This equation, when modified to include the effect of elevon deflection on drag, will result in an expression of the form

$$C_D = (C_{D_{min}})_{\delta=0} + \frac{\Delta C_{D_{min}}}{\Delta \delta^2} \delta^2 + \frac{dC_D}{dC_L^2} \left\{ C_L - \left[(C_{L_0})_{\delta=0} + \frac{\Delta C_{L_0}}{\Delta \delta} \delta \right] \right\}^2$$

The data from the present test, figure 15, indicate dC_D/dC_L^2 to be some function of δ also. Results of low Mach number tests on this same configuration reported in reference 12 show that dC_D/dC_L^2 is approximately a linear function of δ . In the absence of any other evidence, it is assumed that this result would be independent of Mach number. Hence,

$$C_D = (C_{D_{min}})_{\delta=0} + \frac{\Delta C_{D_{min}}}{\Delta \delta^2} \delta^2 + \left[\frac{dC_D}{dC_L^2} + \frac{\Delta (dC_D/dC_L^2)}{\Delta \delta} \delta \right] \left\{ C_L - \left[(C_{L_0})_{\delta=0} + \frac{\Delta C_{L_0}}{\Delta \delta} \delta \right] \right\}^2$$

which should apply at least within the range of elevon deflections used in this test. The parameters $\Delta C_{D_{min}}/\Delta \delta^2$, $\Delta C_{L_0}/\Delta \delta$, and $\frac{\Delta (dC_D/dC_L^2)}{\Delta \delta}$ are presented in figure 18 as determined from the test data. The results in figures 15 and 18 are applicable only within the range of lift coefficients covered in the test.

Hinge Moments

Effect of elevon deflection on hinge moment.- The variation of hinge-moment coefficient with elevon deflection $C_{h\delta}$ is given as a function of Mach number in figure 19. At subsonic speeds, $C_{h\delta}$ increases sharply and reaches a maximum magnitude of 0.045 at approximately $M = 1.0$.

Effect of angle of attack on hinge moment.- The variation of hinge-moment coefficient with angle of attack $C_{h\alpha}$ is plotted in figure 20 for the Mach numbers covered in the test. The variation is similar to that of $C_{h\delta}$ with the maximum value of -0.027 occurring at $M = 1.1$ for neutral elevon, and about -0.03 at $M = 1.3$ for up-elevon deflections.

A comparison of the values of $C_{h\delta}$ and $C_{h\alpha}$ determined from the present test with those obtained in reference 1 is presented in figures 19 and 20. Some of the differences in values of $C_{h\alpha}$ and $C_{h\delta}$ between the tests may be attributed to nonlinearities. The data indicate that C_h may be nonlinear with α above 6° at $M = 1.0$. There is also the possibility that $C_{h\alpha}$ may be nonlinear with δ .

Basic hinge-moment coefficient.- The change in the basic hinge-moment coefficient C_{h0} with Mach number is given in figure 21. The absolute values presented from the present test are questionable because of inaccuracies in measuring small hinge moments. Comparison with the data of reference 1 shows general agreement in shape, but not in magnitude.

Static Longitudinal Stability

The measured periods P of the short-period longitudinal oscillations in angle of attack resulting from the abrupt movement of the elevons were used in determining the static-stability parameters presented herein. The variation of period with Mach number is presented in figure 22. From this figure it can be seen that the period decreased sharply at transonic speeds with the expected more gradual decrease at supersonic speeds; also, different values were obtained for neutral- and up-elevon conditions.

The values of period were used to calculate (for the elevon-fixed condition) the static longitudinal stability parameter $C_{m\alpha}$, which is shown as a function of Mach number in figure 23(a). The reduced frequency

parameter $k = \frac{\omega \bar{c}}{2V}$ equalled 0.025 within ± 8 percent throughout the Mach number range.

The aerodynamic-center location (fig. 23(b)) throughout the Mach number range from 0.88 to 1.70 was computed from C_{m_α} and C_{L_α} . The nonlinearities in the lift and pitching moments produced the two curves for aerodynamic center as shown in figure 23(b). The aerodynamic center with the elevon neutral moves from the most forward location of 41.0 percent mean aerodynamic chord at $M = 0.88$ to the most rearward location of 52.0 percent mean aerodynamic chord at $M = 1.37$ followed by a gradual forward movement to 48.0 percent mean aerodynamic chord at $M = 1.65$. The movement of the aerodynamic center is similar when the elevon is deflected -9° . A comparison of the results of the present test with those of reference 1 (shown in fig. 23) shows fair agreement over the Mach number range tested.

Damping in Pitch

The damping-in-pitch parameters $T_{1/2}$ (the time required to damp to half amplitude), and $C_{m_{\theta \bar{c}}} + C_{m_{\dot{\alpha} \bar{c}}}$ (fig. 24) are determined by an analysis of the rate of decay of the short-period longitudinal oscillations induced by the abrupt movement of the elevons. These damping parameters indicate the model was dynamically longitudinally stable for the Mach number range presented. The values of $C_{m_{\theta \bar{c}}} + C_{m_{\dot{\alpha} \bar{c}}}$ obtained in reference 1 are shown plotted in figure 24(b). The agreement with previous data appears to be good over the small Mach number range where comparisons can be made.

Longitudinal-Control Effectiveness

The effectiveness of the constant-chord full-span elevon in producing lift and pitching moment is given in figure 25. The change in lift coefficient per degree of elevon deflection C_{L_δ} shows a gradual variation with Mach number from a maximum value of 0.019 at $M = 0.9$ to 0.0055 at $M = 1.7$.

The pitching-effectiveness parameter C_{m_δ} (fig. 25(b)) remained negative throughout the Mach number range covered by the test, although the pitching effectiveness was reduced at supersonic speeds.

Two more longitudinal-control effectiveness parameters (discussed more fully in the appendix of reference 1), the change in trim angle of attack per degree of elevon deflection $\left(\frac{\Delta\alpha}{\Delta\delta}\right)_{\text{trim}}$ and the rate of change in trim lift coefficient with elevon deflection $(C_{L\delta})_{\text{trim}}$, are presented as functions of Mach number in figures 26(a) and (b). Both of these figures serve to show the reduction in control effectiveness at transonic and supersonic speeds.

A summary of these longitudinal-control effectiveness parameters indicates the elevon was an effective control within the Mach number range tested. Comparisons of the control effectiveness parameters from reference 1 with those discussed in the preceding section show good agreement.

Longitudinal Trim

The basic pitching-moment coefficient C_{m_0} at zero angle of attack and zero elevon deflection is shown as a function of Mach number in figure 27. The trim change was mild with the model tending to trim at small negative values of angle of attack below $M = 1.01$ and small positive values above $M = 1.01$. The out-of-trim moments reached a maximum at $M = 1.2$ and gradually decreased to approximately zero at $M = 1.7$. The shape of the curve obtained from this test is quite similar to that reported in reference 1 (also shown in fig. 27), although there are some differences in absolute values.

CONCLUSIONS

From an analysis of the results of the flight test of a rocket-powered model of a tailless delta wing (60° leading-edge sweepback) airplane configuration from $M = 0.75$ to $M = 1.70$, the following conclusions are indicated:

1. The variation of lift-curve slope C_{L_α} with Mach number M is gradual with a maximum value of 0.054 near $M = 1.0$.
2. Buffeting is not encountered at low and moderate lift coefficients within the speed range covered, although it is observed at high subsonic speeds near the maximum lift coefficient attained.

3. The drag rise occurs at approximately $M = 0.90$; the greatest minimum drag coefficient is about 0.040 at $M = 1.15$.

4. Deflecting the elevator up approximately 9° produces an increase in the minimum drag coefficient of about 0.005 at $M = 1.6$.

5. The resultant-force vector with elevon neutral at all speeds and at low lift coefficients is inclined forward from the normal to the plane of the wing. Deflecting the elevon up 9° rotates the vector behind this reference at all but the lowest Mach numbers.

6. The maximum lift-drag ratio ranges from 9.0 to about 7.6 at high subsonic speeds with neutral elevon; deflecting the elevon up 9° reduces it by a factor of three-fourths to one-half.

7. The hinge-moment coefficient per degree of elevon deflection $C_{h\delta}$ increases sharply at subsonic speeds and reaches a maximum value of -0.045 at $M = 1.0$. The hinge-moment coefficient per degree of angle of attack $C_{h\alpha}$ exhibits a similar variation with Mach number, reaching a maximum value of -0.027 at $M = 1.1$ for neutral elevon and -0.030 at $M = 1.3$ for 9° up elevon.

8. The elevon is an effective control throughout the Mach number range covered by the test, although the effectiveness is reduced to about one-half of its subsonic value at supersonic speeds.

9. The transonic trim change is mild.

10. The aerodynamic-center location with elevon neutral shows a gradual rearward movement from 41 percent mean aerodynamic chord at $M = 0.88$ to 52 percent mean aerodynamic chord at $M = 1.37$ and forward to 48 percent mean aerodynamic chord at $M = 1.65$.

11. The damping parameters and coefficients indicated that the configuration is dynamically longitudinally stable throughout the test Mach number range.

Langley Aeronautical Laboratory
National Advisory Committee for Aeronautics
Langley Field, Va.

REFERENCES

1. Mitcham, Grady L., Stevens, Joseph E., and Norris, Harry P.: Aerodynamic Characteristics and Flying Qualities of a Tailless Triangular-Wing Airplane Configuration As Obtained from Flights of Rocket-Propelled Models at Transonic and Low Supersonic Speeds. NACA RM L9L07, 1950.
2. Mitchell, Jesse L., and Peck, Robert F.: An NACA Vane-Type Angle-of-Attack Indicator for Use at Subsonic and Supersonic Speeds. NACA RM L9F28a, 1949.
3. Gillis, Clarence L., Peck, Robert F., and Vitale, A. James: Preliminary Results from a Free-Flight Investigation at Transonic and Supersonic Speeds of the Longitudinal Stability and Control Characteristics of an Airplane Configuration with a Thin Straight Wing of Aspect Ratio 3. NACA RM L9K25a, 1950.
4. Gillis, Clarence L., and Vitale, A. James: Wing-On and Wing-Off Longitudinal Characteristics of an Airplane Configuration Having a Thin Unswept Tapered Wing of Aspect Ratio 3, as Obtained from Rocket-Propelled Models at Mach Numbers from 0.8 to 1.4. NACA RM L50K16, 1951.
5. Brown, Clinton E.: Theoretical Lift and Drag of Thin Triangular Wings at Supersonic Speeds. NACA Rep. 839, 1946. (Formerly NACA TN 1183.)
6. Spreiter, John R.: The Aerodynamic Forces on Slender Plane- and Cruciform-Wing and Body Combinations. NACA Rep. 962, 1950.
7. Gillis, Clarence L.: Buffeting Information Obtained from Rocket-Propelled Airplane Models Having Thin Unswept Wings. NACA RM L50H22a, 1950.
8. Mitcham, Grady L., and Blanchard, Willard S., Jr.: Summary of the Aerodynamic Characteristics and Flying Qualities Obtained from Flights of Rocket-Propelled Models of an Airplane Configuration Incorporating a Sweptback Inversely Tapered Wing at Transonic and Low-Supersonic Speeds. NACA RM L50G18a, 1950.
9. Purser, Paul E.: Notes on Low-Lift Buffeting and Wing Dropping at Mach Numbers near 1. NACA RM L51A30, 1951.
10. Lauten, William T., Jr., and Mitcham, Grady L.: Note on Flutter of a 60° Delta Wing Encountered at Low-Supersonic Speeds during the Flight of a Rocket-Propelled Model. NACA RM L51B28, 1951.

11. Karpovich, E. A., and Frankl, F. I.: Resistance of a Delta Wing in a Supersonic Flow. NACA TM 1283, 1951.
12. Wolhart, Walter D., and Michael, William H., Jr.: Wind-Tunnel Investigation of the Low-Speed Longitudinal and Lateral Control Characteristics of a Triangular-Wing Model of Aspect Ratio 2.31 Having Constant-Chord Control Surfaces. NACA RM L50G17, 1950.

TABLE I

PHYSICAL CHARACTERISTICS OF A DELTA-WING, TAILLESS

AIRPLANE CONFIGURATION

Wing:

Area, sq ft (included)	6.25
Span, ft	3.80
Aspect ratio	2.31
Mean aerodynamic chord, ft	2.19
Sweepback of leading edge, deg	60
Dihedral (relative to mean thickness line), deg	0
Taper ratio (Tip chord/Root chord)	0
Airfoil section	NACA 65(06)A006.5

Vertical tail:

Area (outside of fuselage), sq ft	0.81
Height (outside of fuselage), ft	0.97
Sweepback of leading edge, deg	60
Taper ratio (Tip chord/Root chord)	0
Airfoil section	NACA 65(06)A006.5

Elevon:

Type	Plain flap
Area (aft of hinge line, one), sq ft	0.51
Span (at trailing edge of wing, one), ft	1.78
Chord (hinge line to trailing edge), ft	0.37

Weight and balance:

Weight, lb	193.4
Wing loading, lb/sq ft	30.94
Center-of-gravity position, percent M.A.C.	20.7
Moment of inertia (I_y), slug-ft ²	17.01



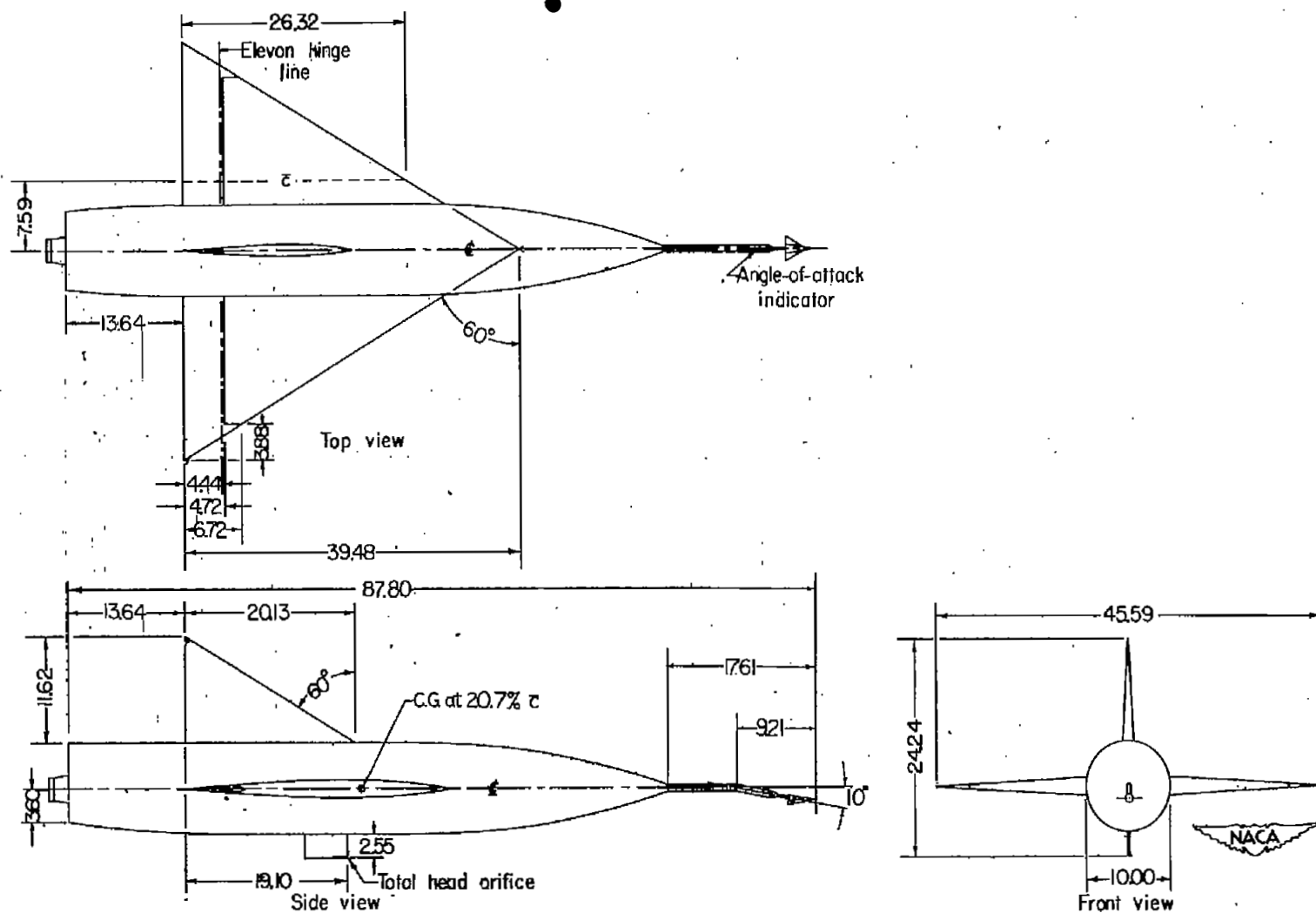


Figure 1.- Three-view drawing of the rocket-powered flight model. (All dimensions are in inches.)

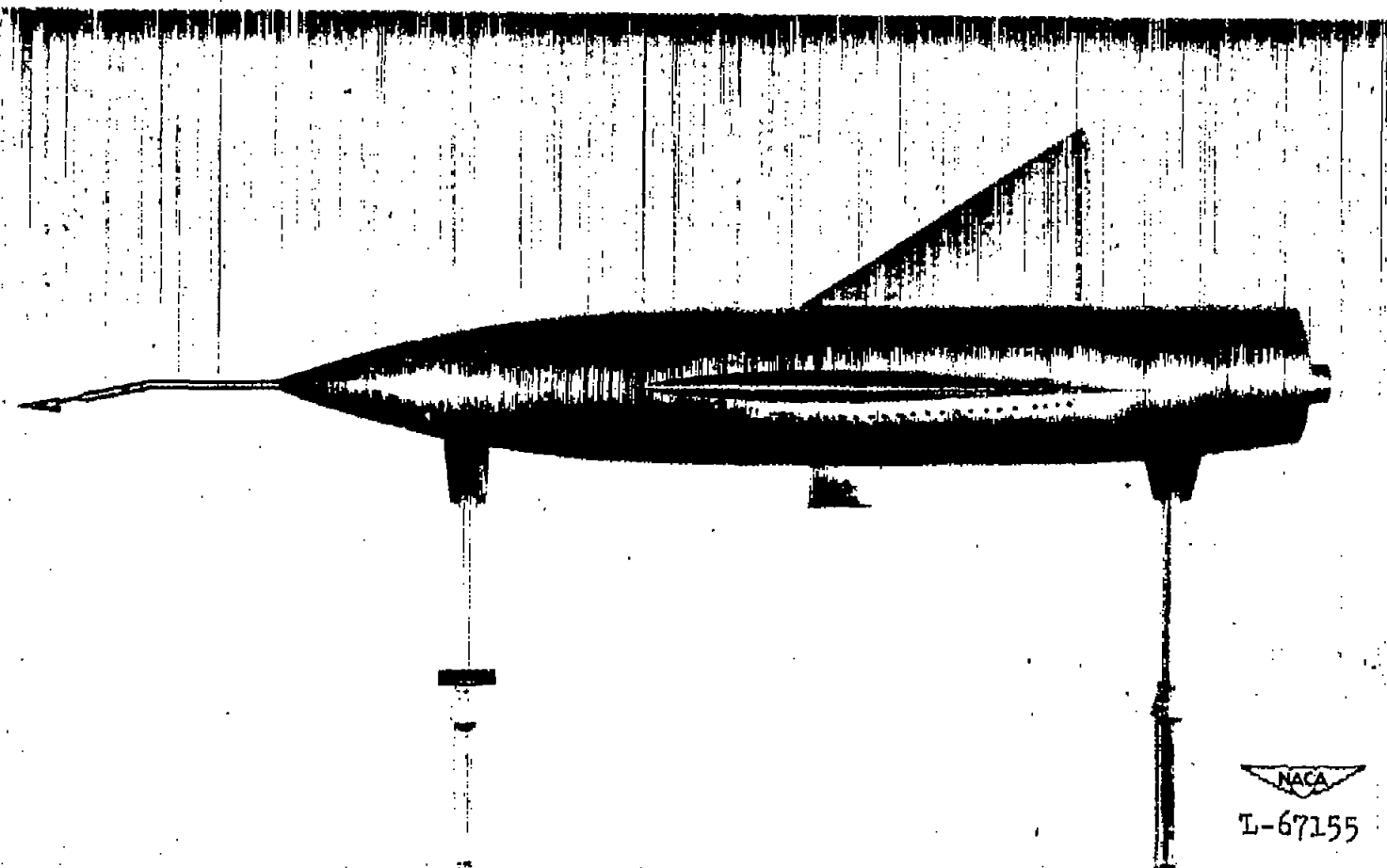


Figure 2.- Side view of the model.

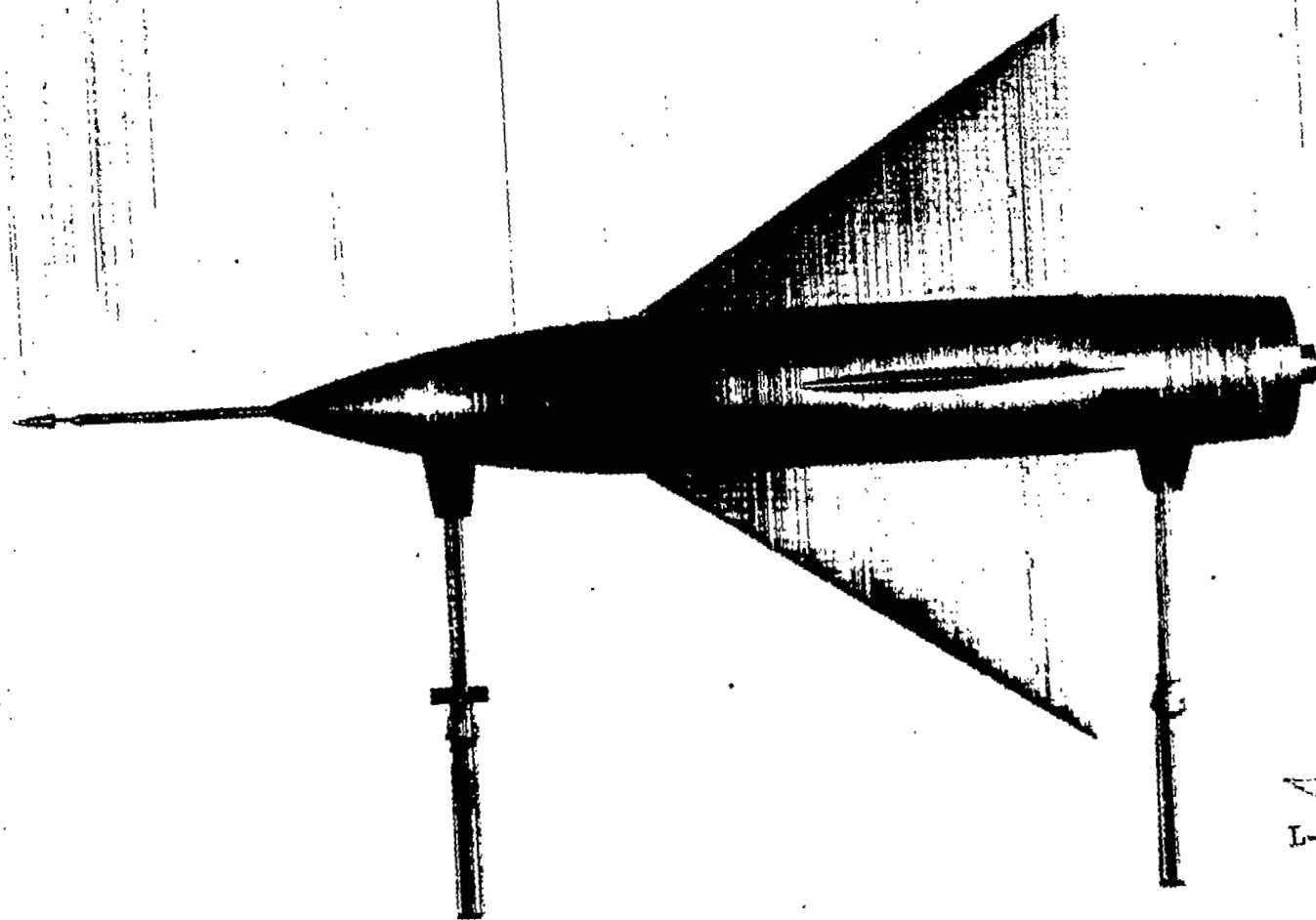


Figure 3.- Top view of the model.

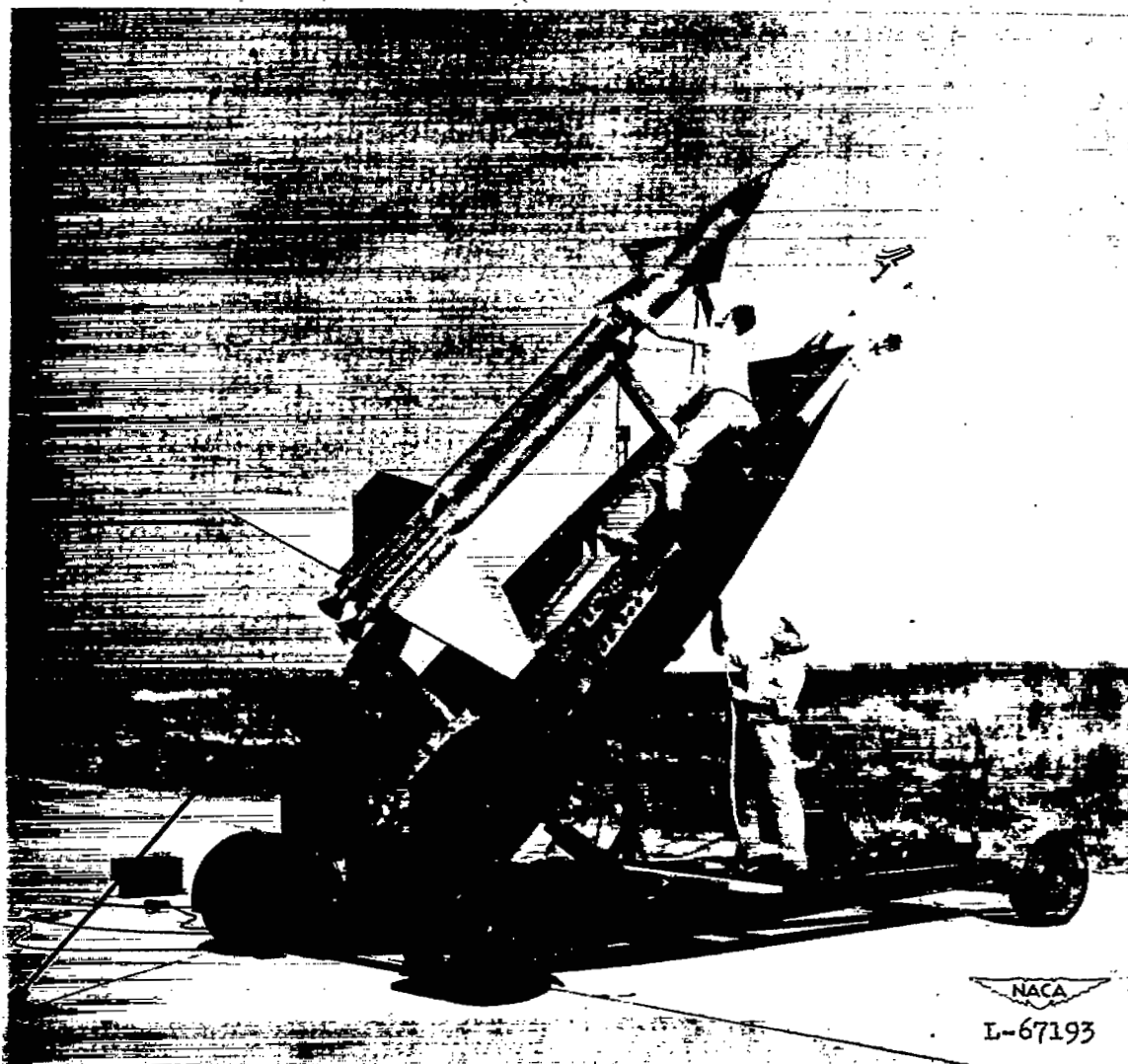


Figure 4.- Booster-model combination on the launcher.

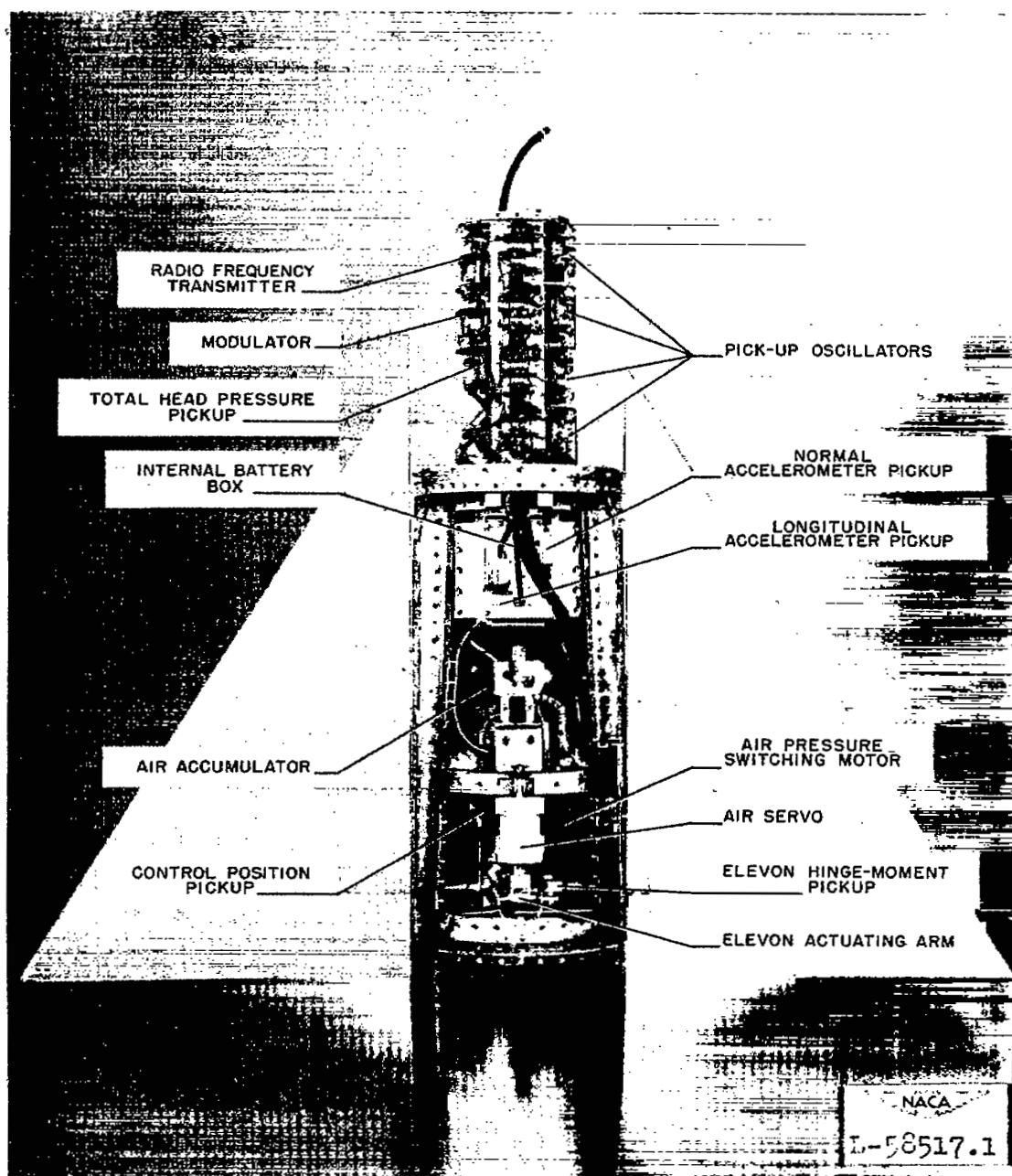


Figure 5.- Disposition of the instrumentation within the model.

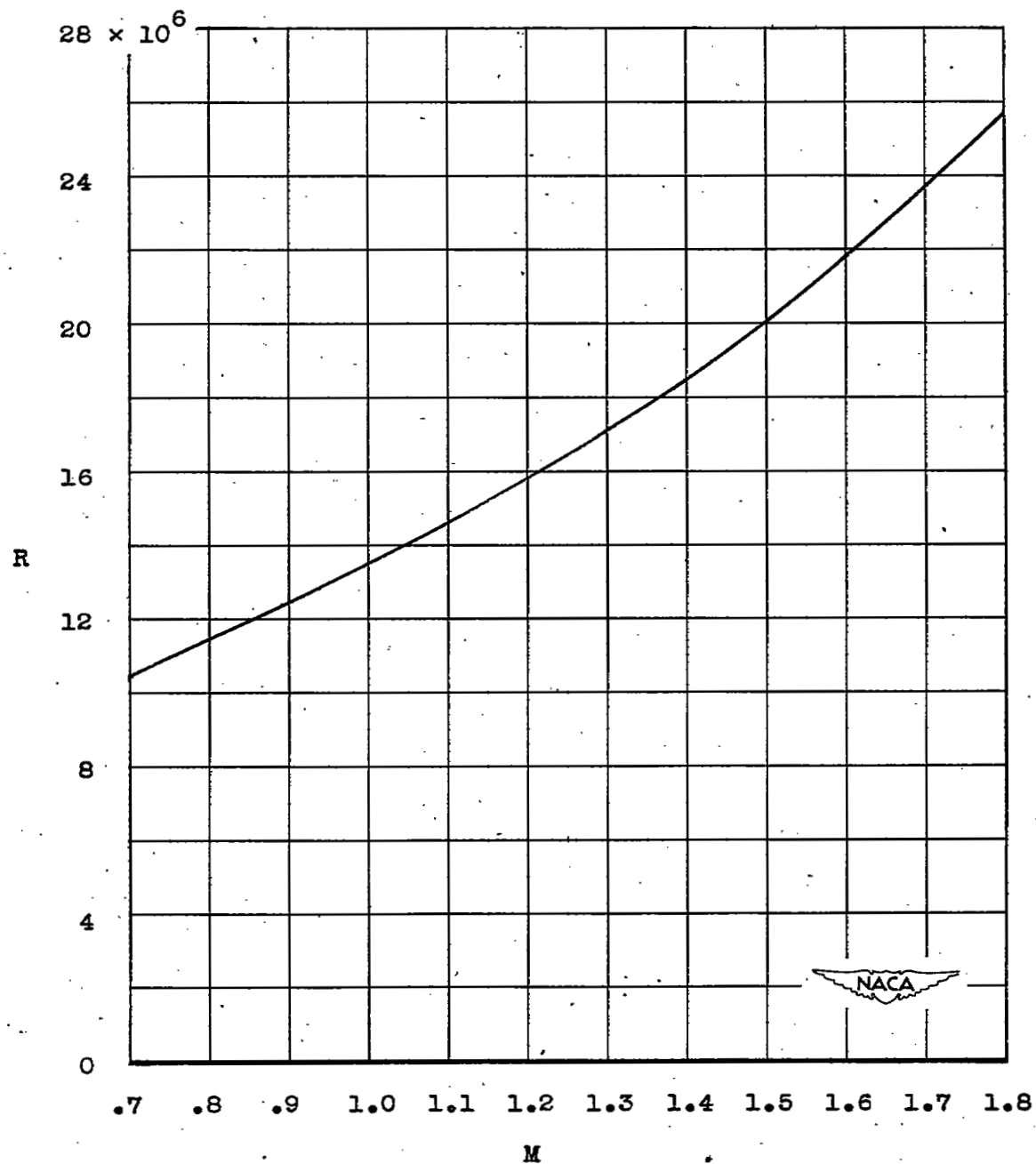


Figure 6.- Reynolds number as a function of Mach number.

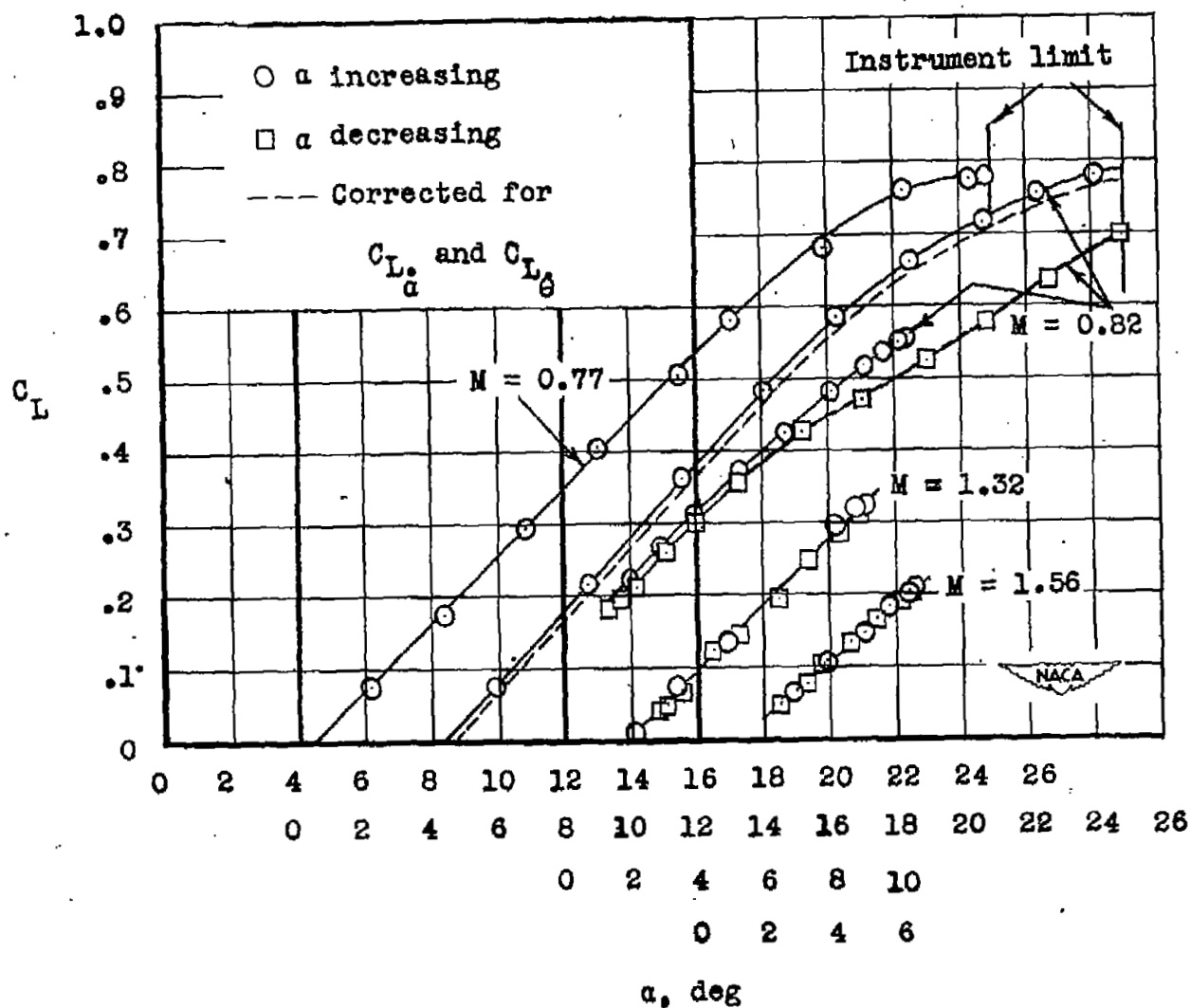


Figure 7.- The effect of angle of attack on lift for several oscillations;
 $\delta = -9^\circ$.

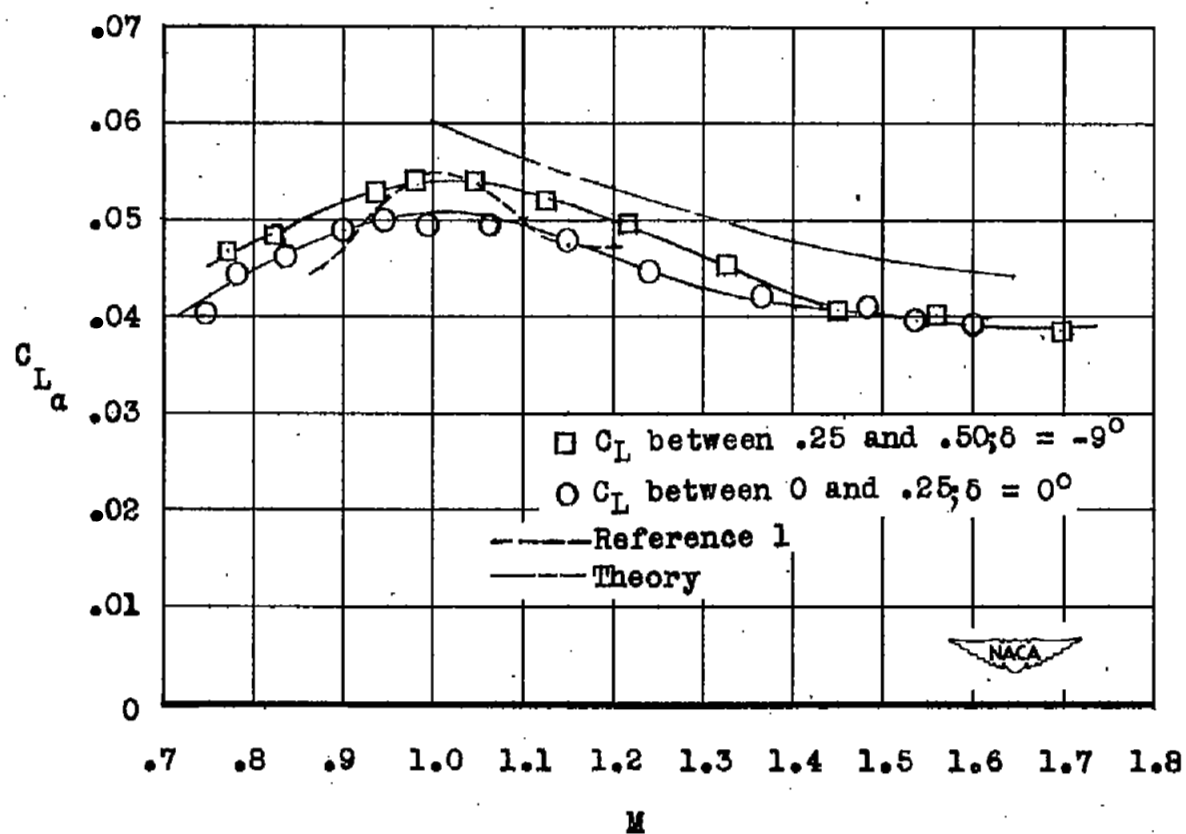


Figure 8.- Lift-curve slope.

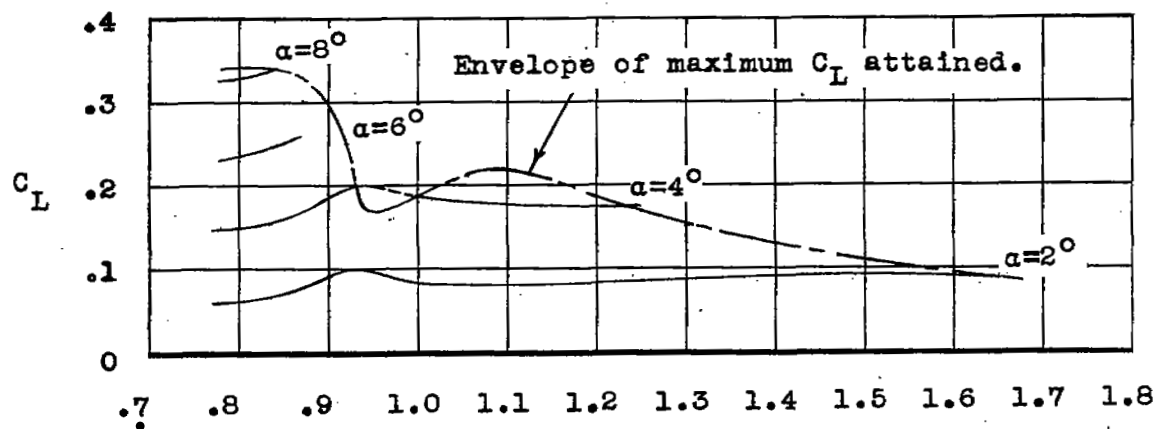
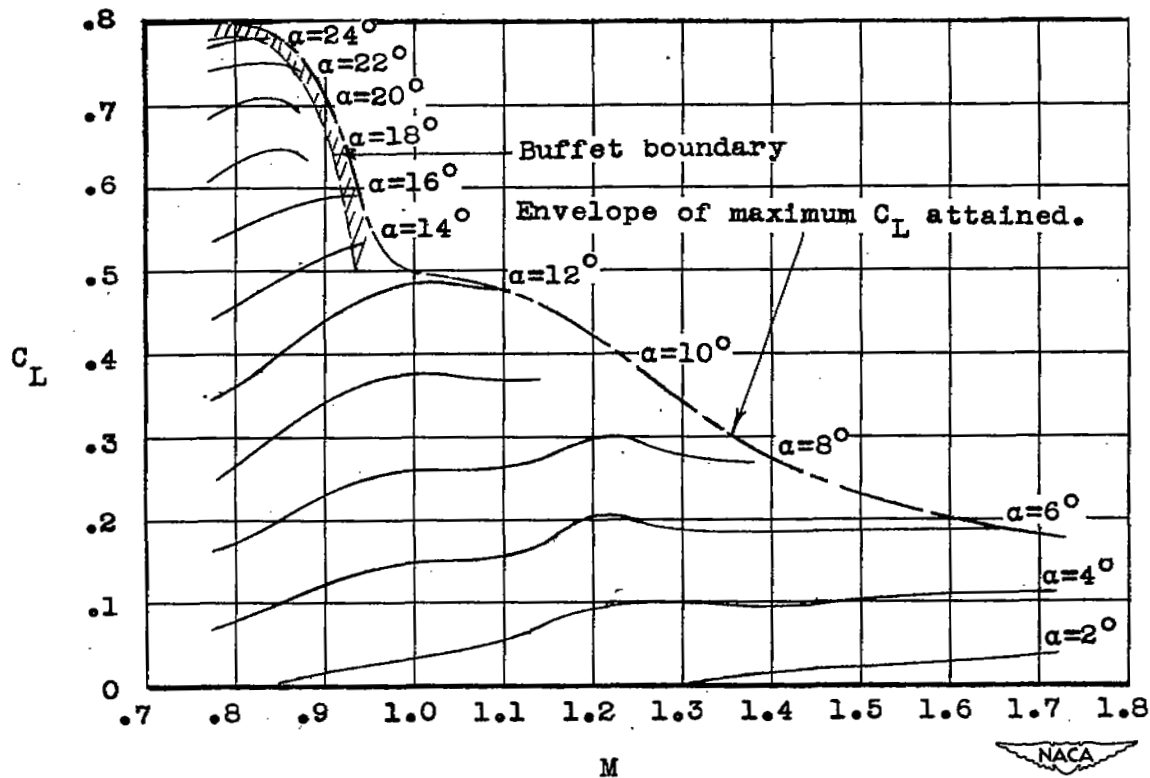
(a) For $\delta_{av} = 0^\circ$.(b) For $\delta_{av} = -9^\circ$.

Figure 9.- Lift and buffet summary.

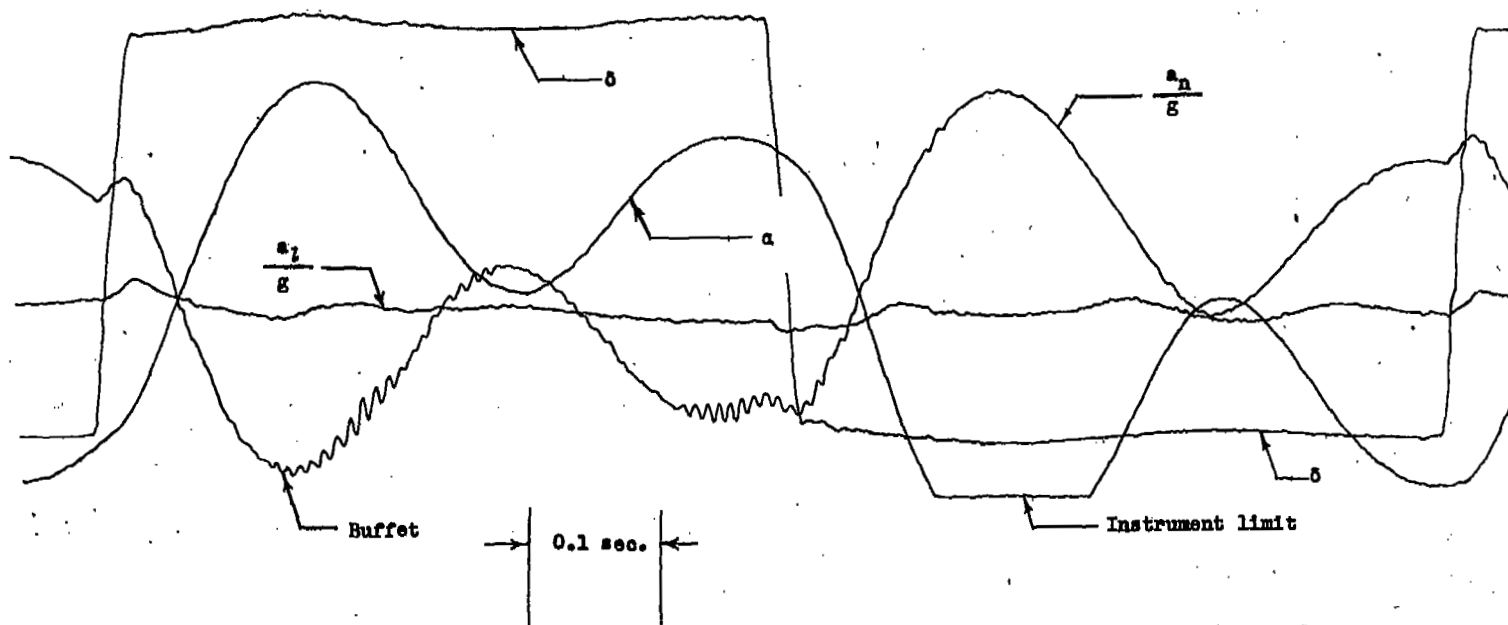


Figure 10.- Section of telemeter record showing buffet.



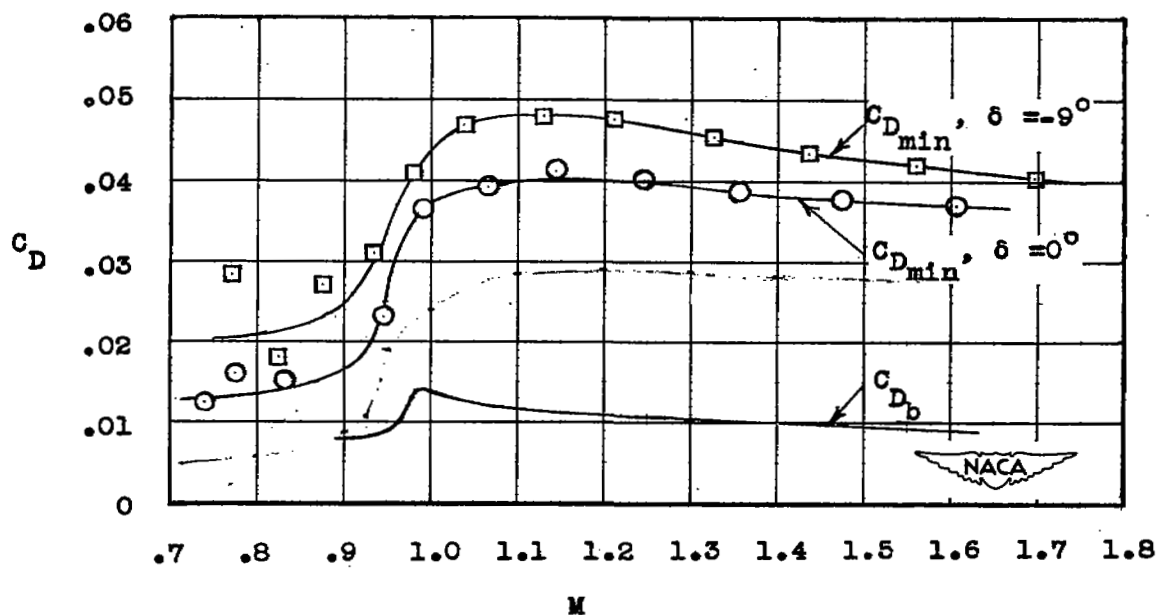


Figure 11.- Minimum and base drag coefficients.

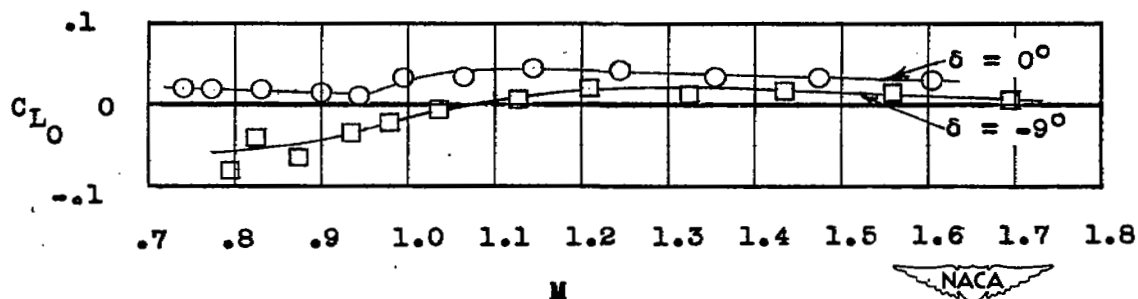


Figure 12.- Lift coefficient for minimum drag.

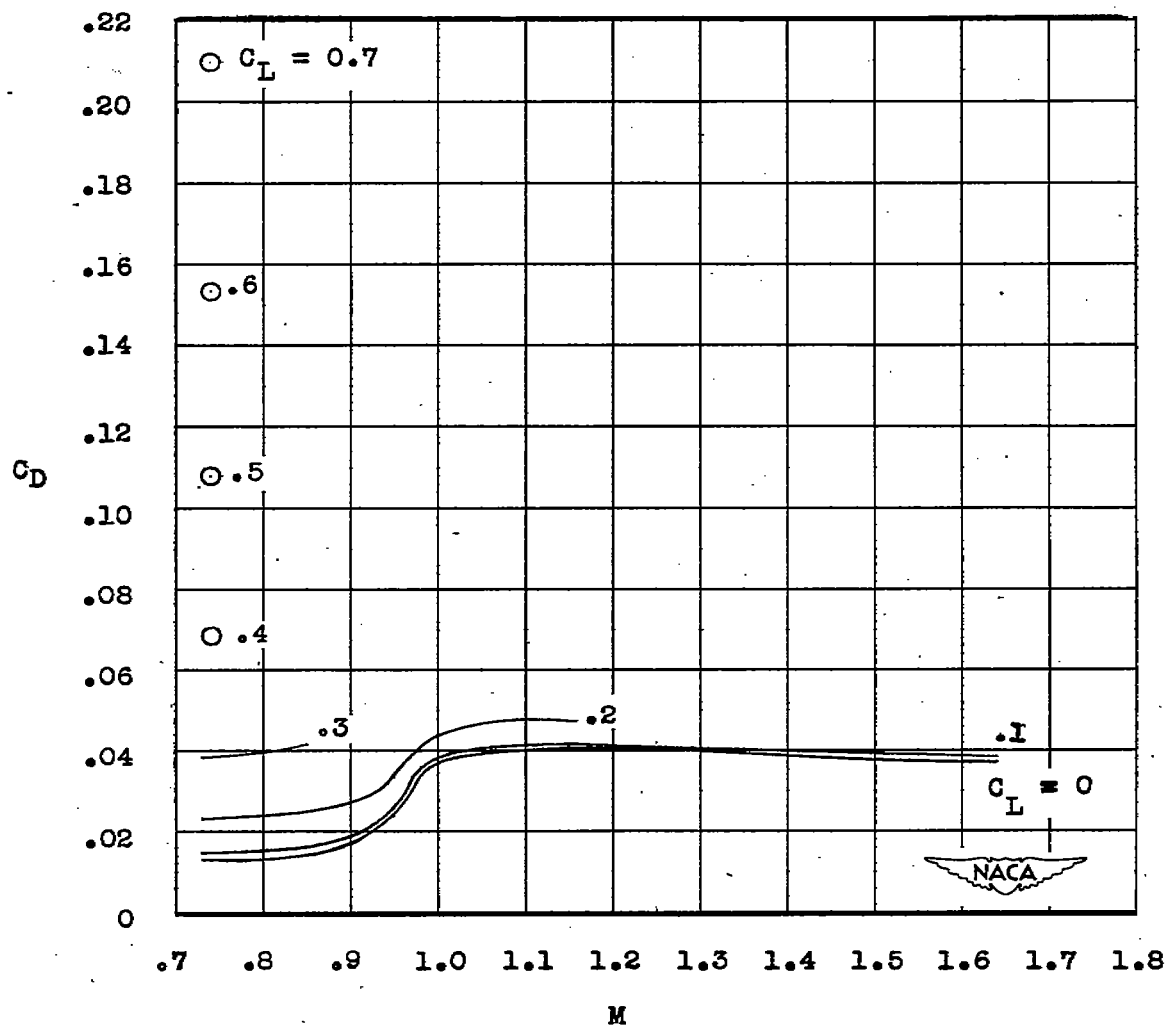


Figure 13.- The variation of drag coefficient with Mach number for various lift coefficients; $\delta_{av} = 0^\circ$.

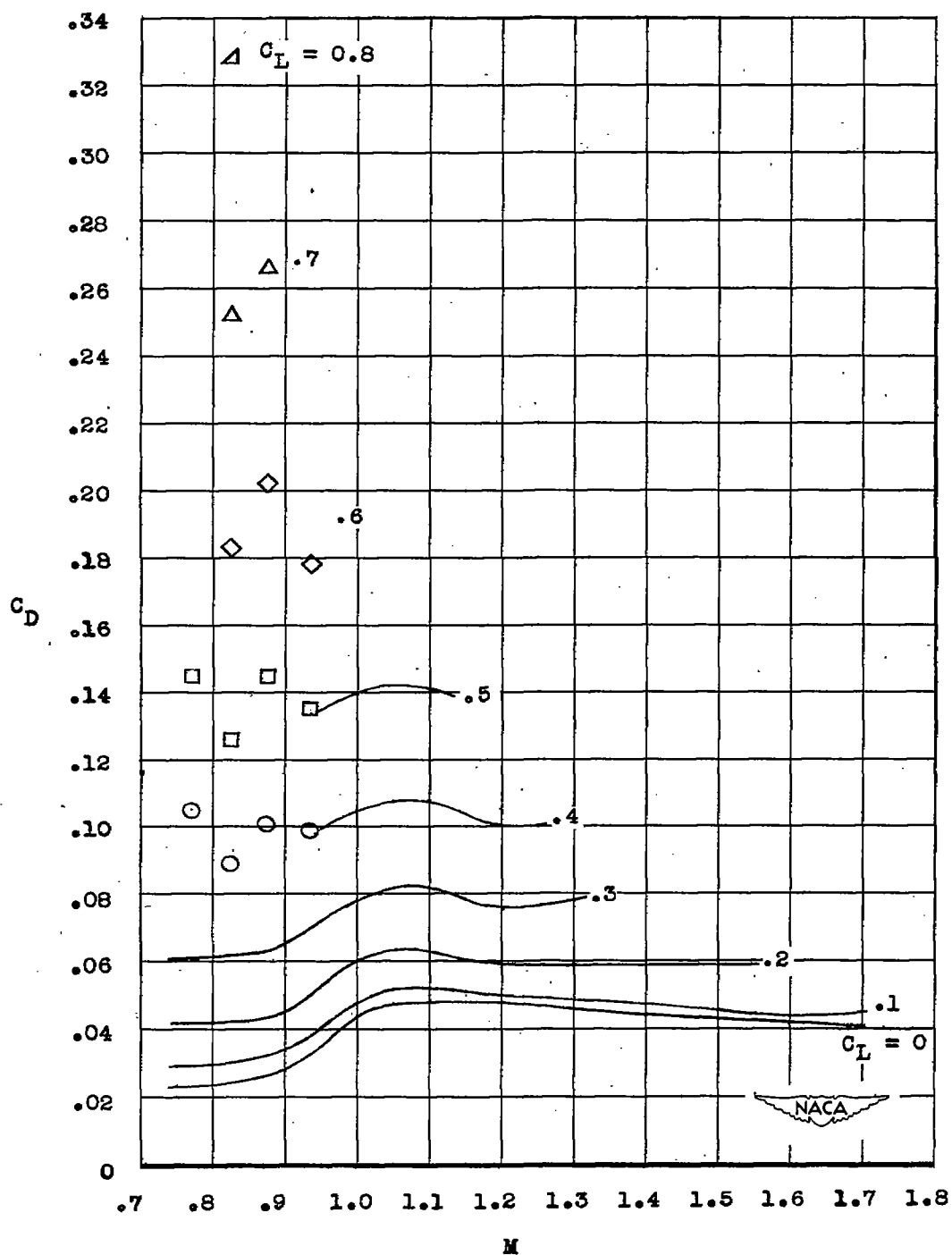
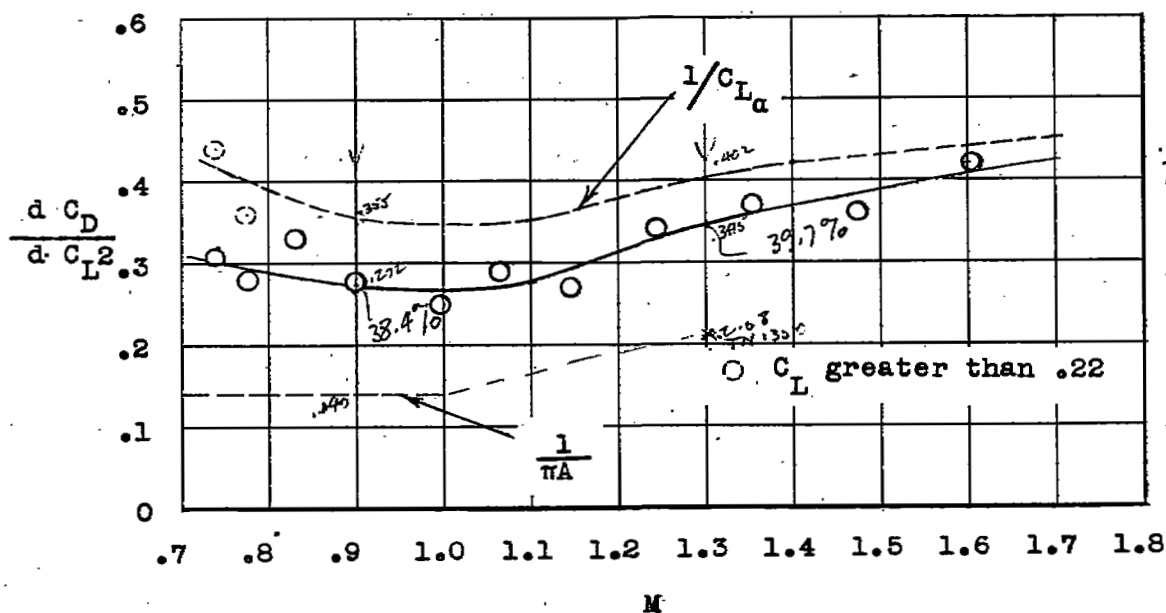
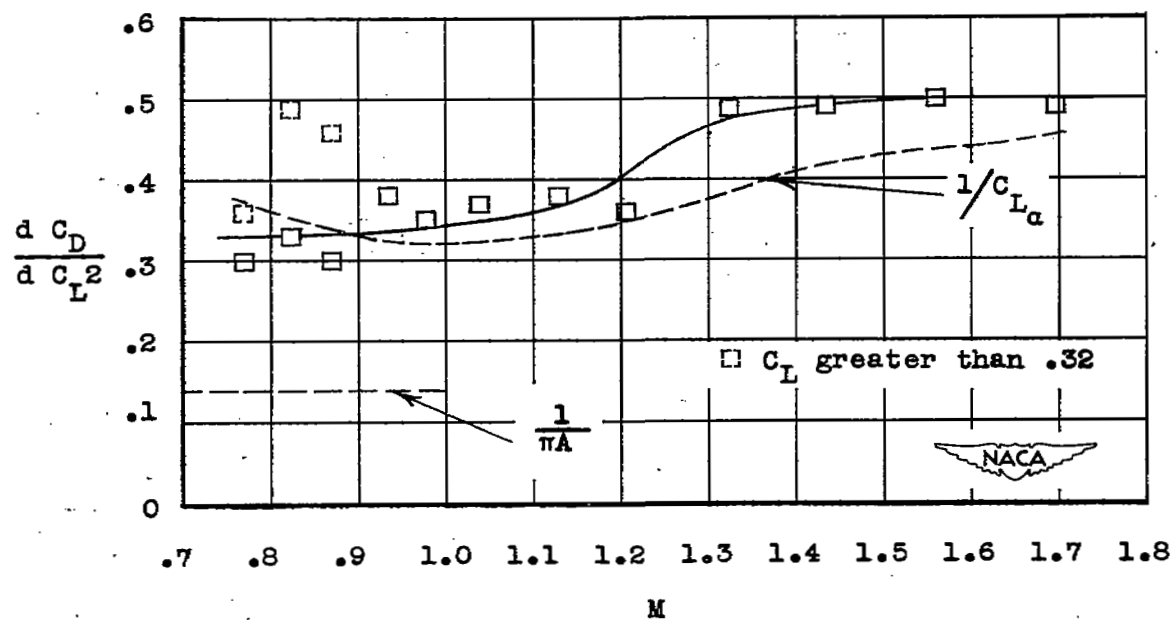


Figure 14.- The variation of drag coefficient with Mach number for various lift coefficients; $\delta_{av} = -9^\circ$.

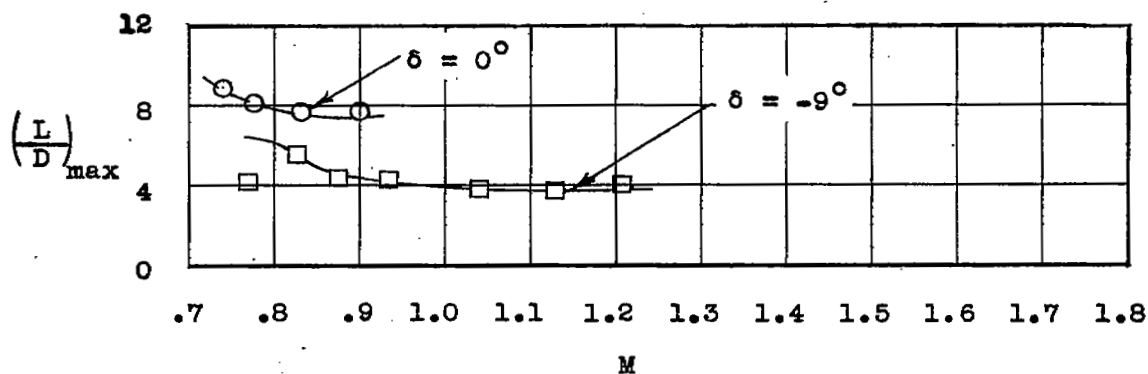


(a) For $\delta_{av} = 0^\circ$.

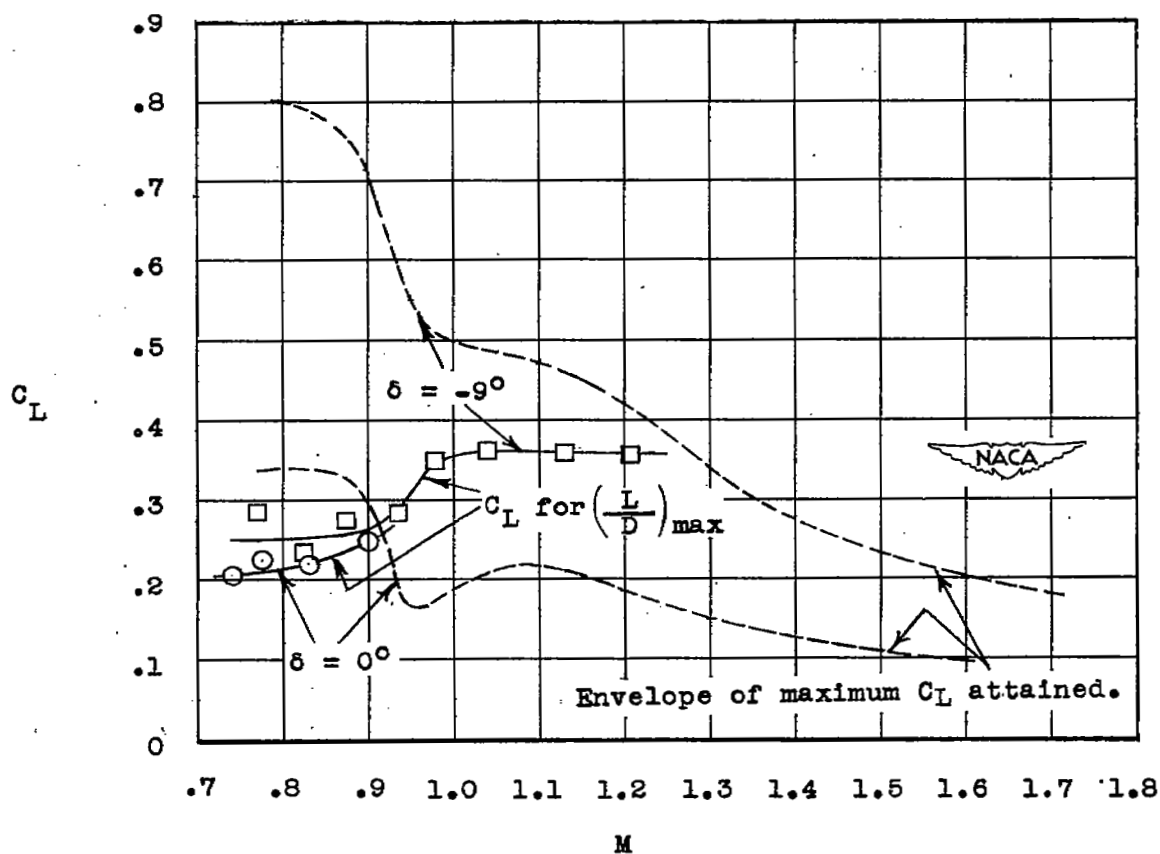


(b) For $\delta_{av} = -9^\circ$.

Figure 15.- The variation of drag parameter dC_D/dC_L^2 with Mach number.



(a) Maximum lift-drag ratios.



(b) Lift coefficient for maximum lift-drag ratio.

Figure 16.- Maximum lift-drag ratio and the lift coefficient for $(L/D)_{\max}$.

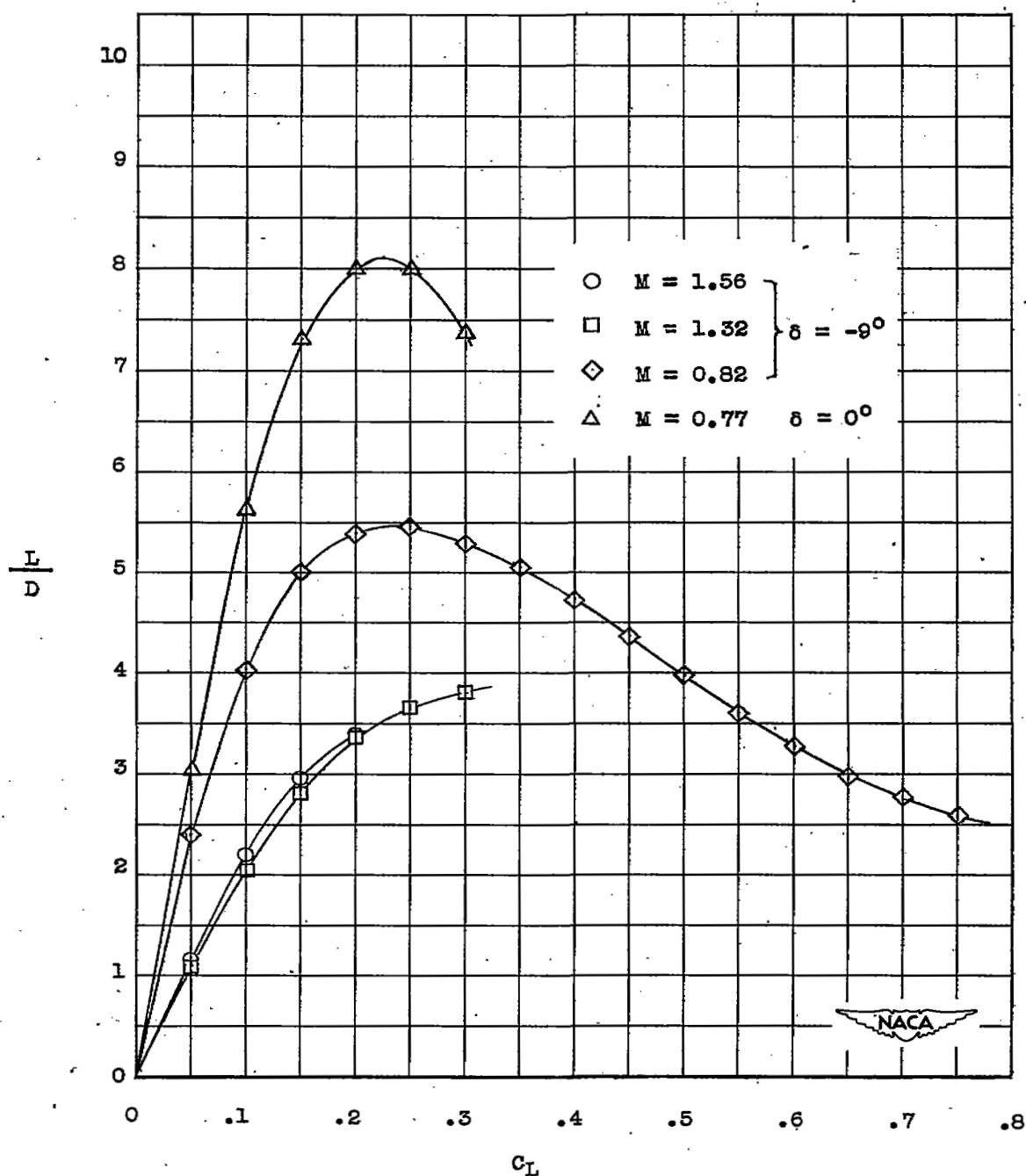
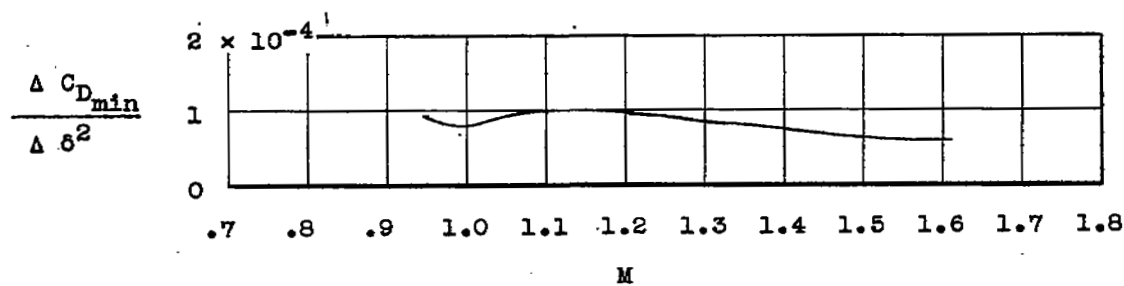
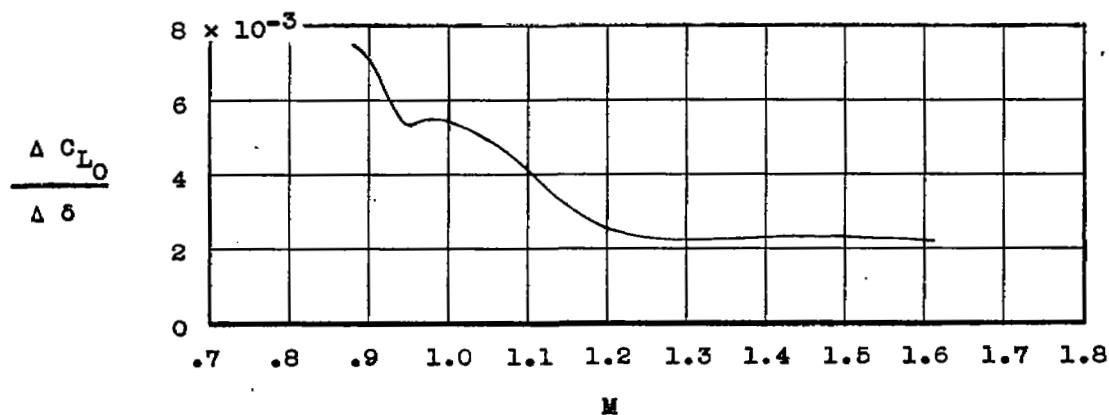


Figure 17.- Lift-drag ratio as a function of lift coefficient for several Mach numbers.



(a) Minimum drag.



(b) Lift coefficient for minimum drag.

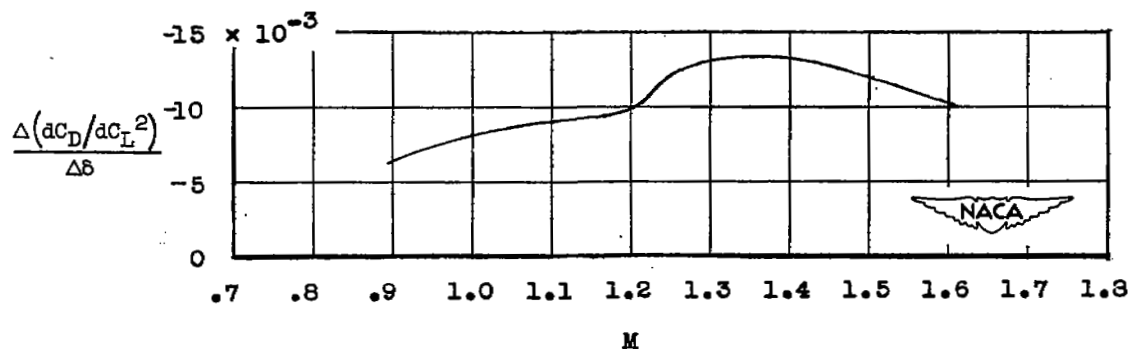
(c) Drag parameter $\frac{\Delta(dC_D/dC_L^2)}{\Delta \delta}$

Figure 18.- Effect of elevon deflection on drag.

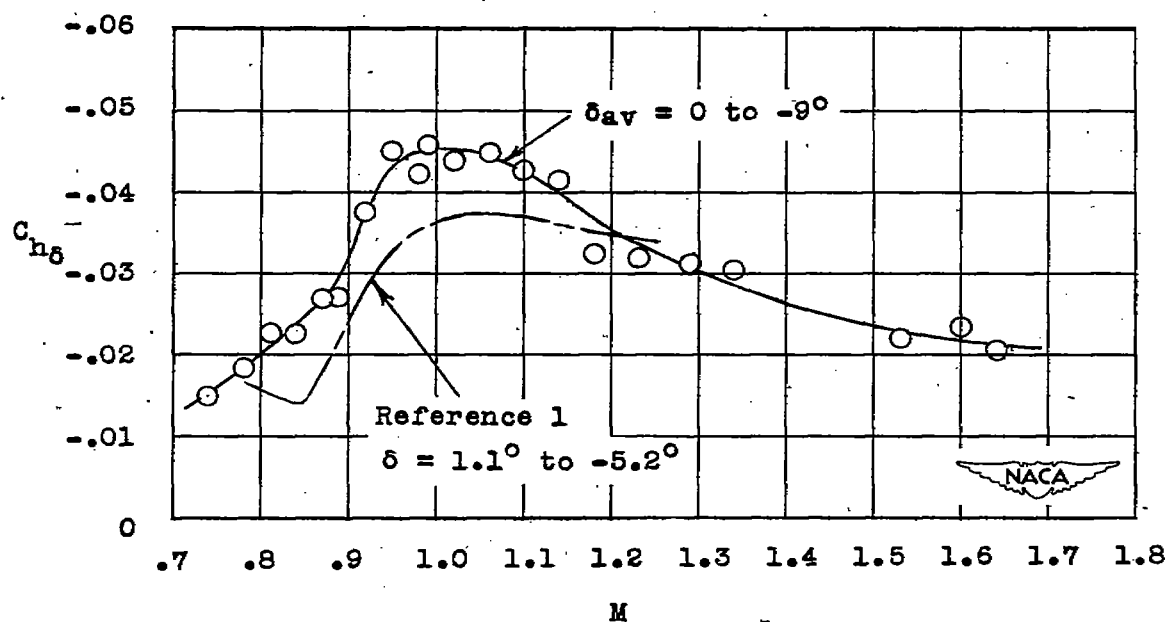


Figure 19.- Effect of Mach number on $C_{h\delta}$.

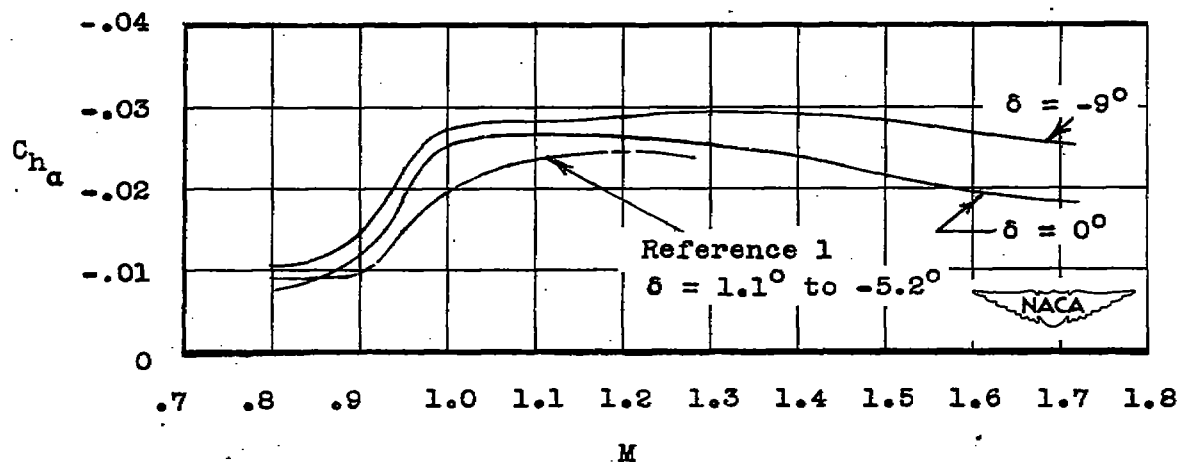


Figure 20.- Effect of Mach number on $C_{h\alpha}$.

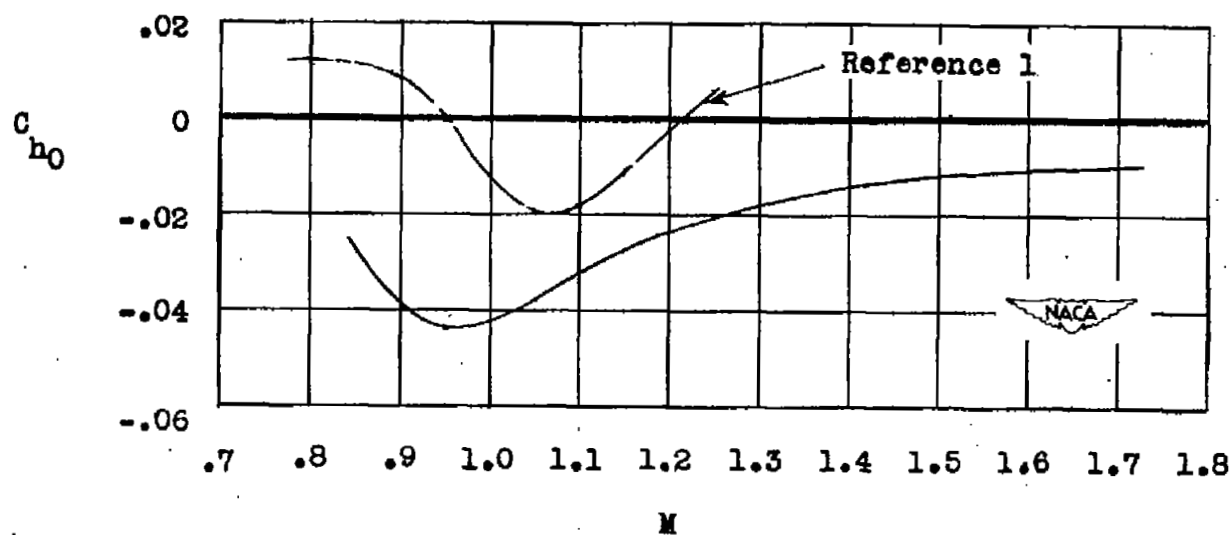


Figure 21.- Basic hinge-moment coefficient.

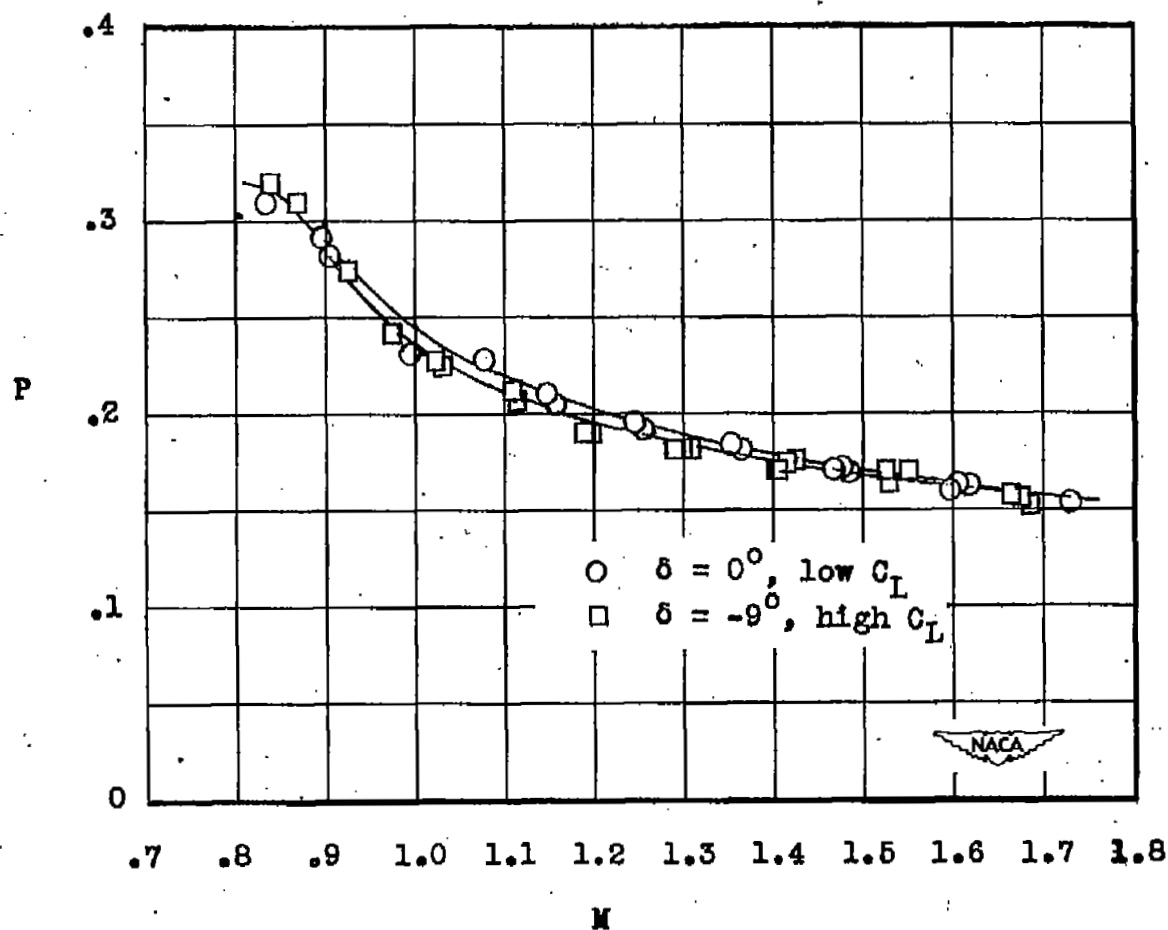
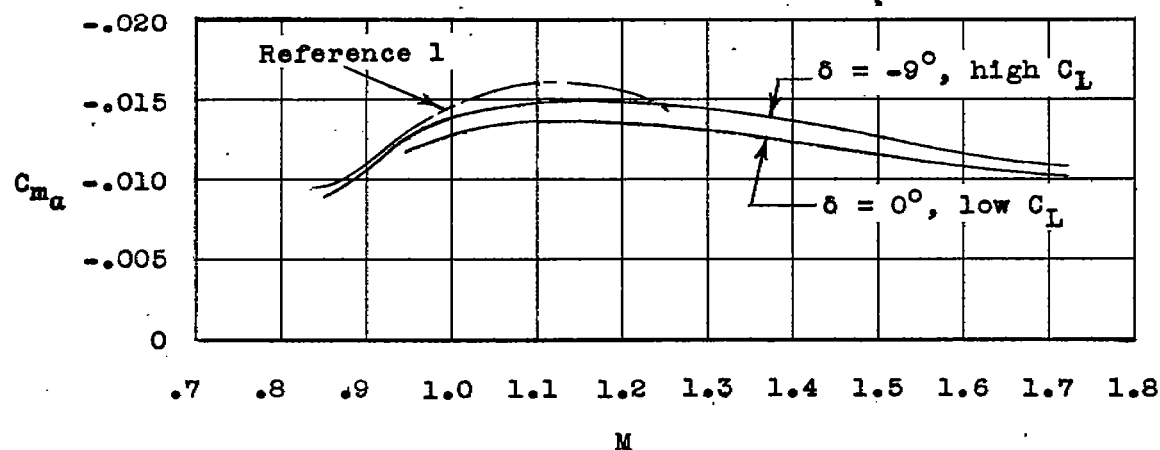
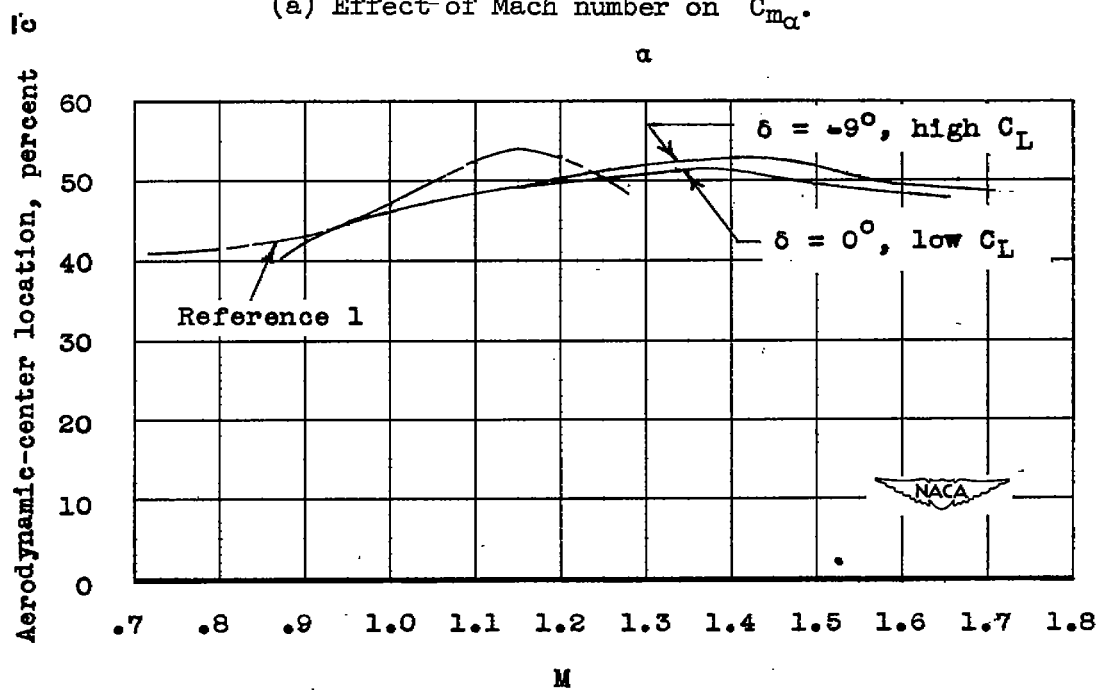
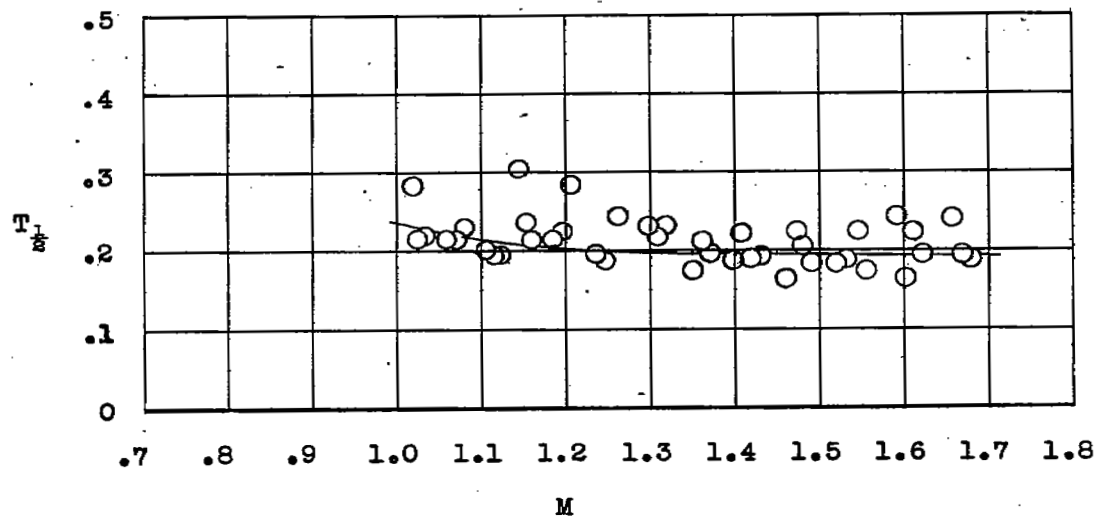


Figure 22.- Period of the longitudinal oscillation.

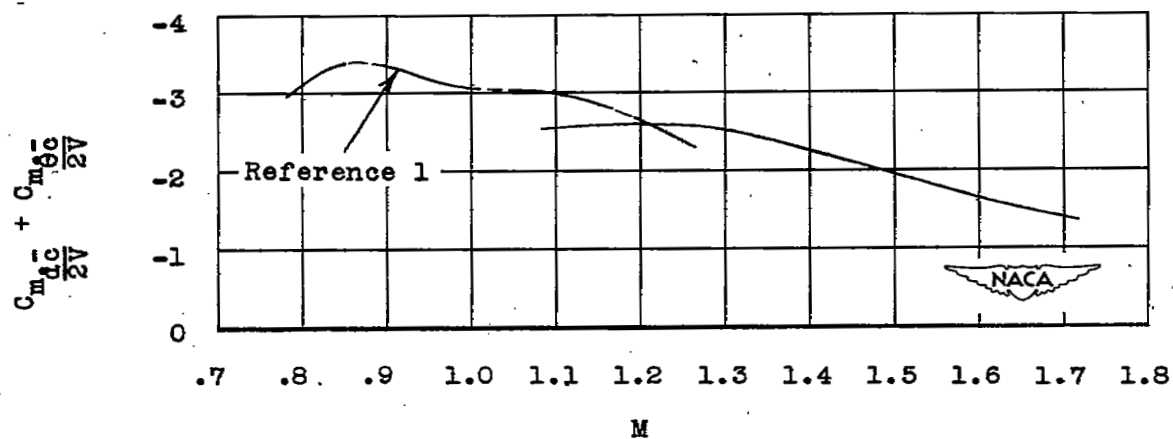
(a) Effect of Mach number on $C_{m\alpha}$.

(b) Effect of Mach number on aerodynamic-center location.

Figure 23.- Longitudinal static stability.

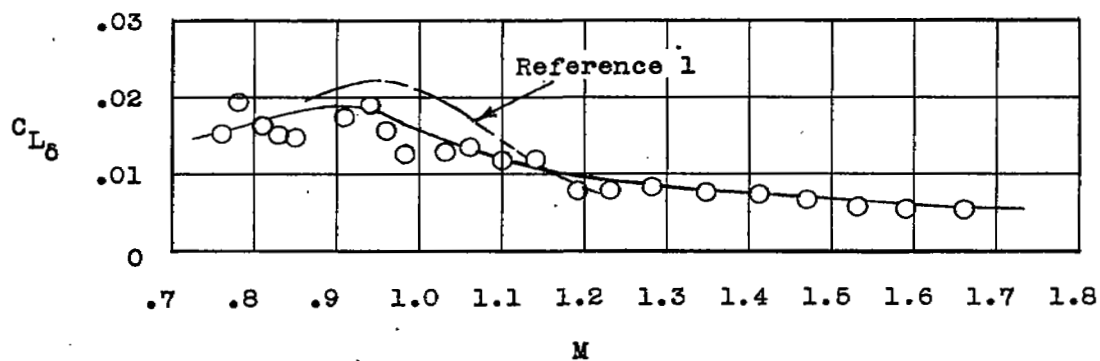


(a) Time to damp to half amplitude.

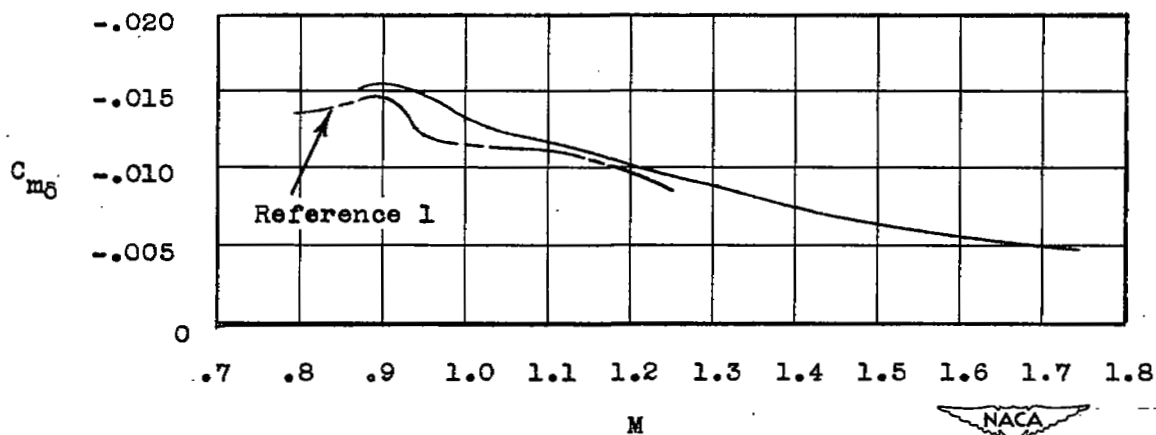


(b) Damping derivatives.

Figure 24.- Damping characteristics of the short-period longitudinal oscillations.

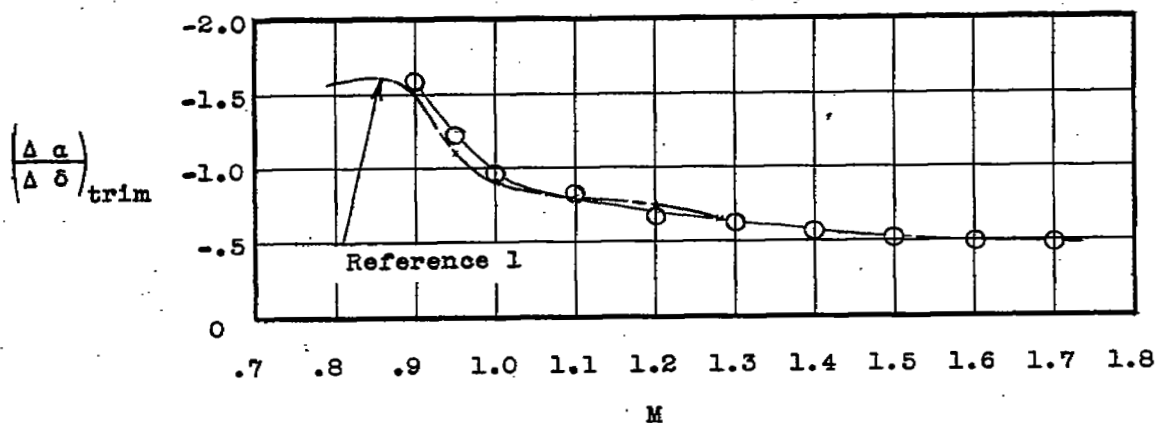


(a) Lift effectiveness.

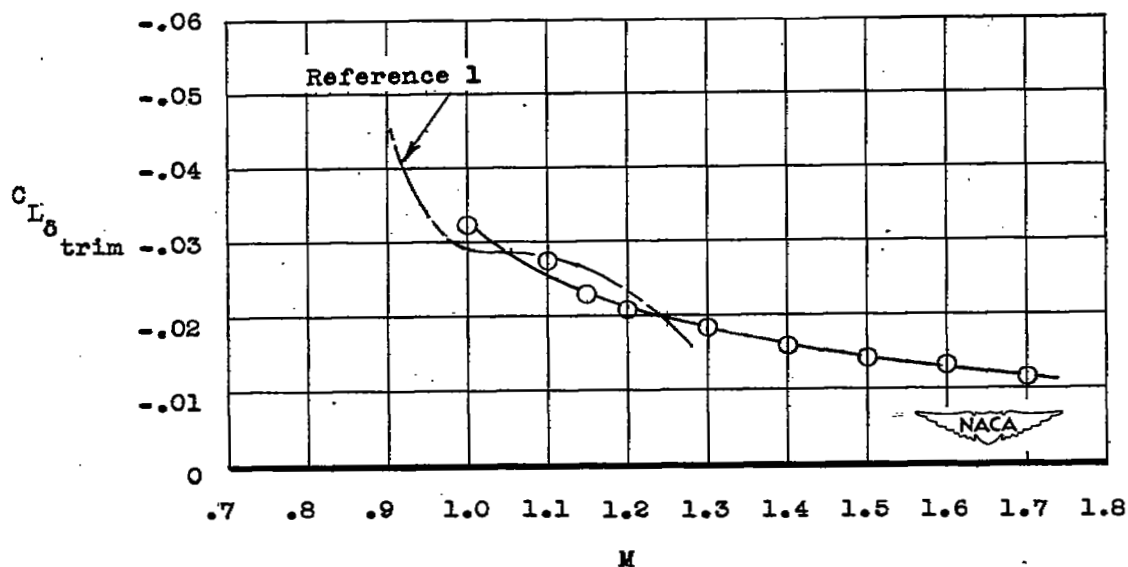


(b) Pitching effectiveness.

Figure 25.- Longitudinal-control effectiveness.



(a) Change in trim angle of attack per degree of elevon deflection.



(b) Trim lift coefficient per degree elevon deflection.

Figure 26.- Longitudinal-control effectiveness for trim.

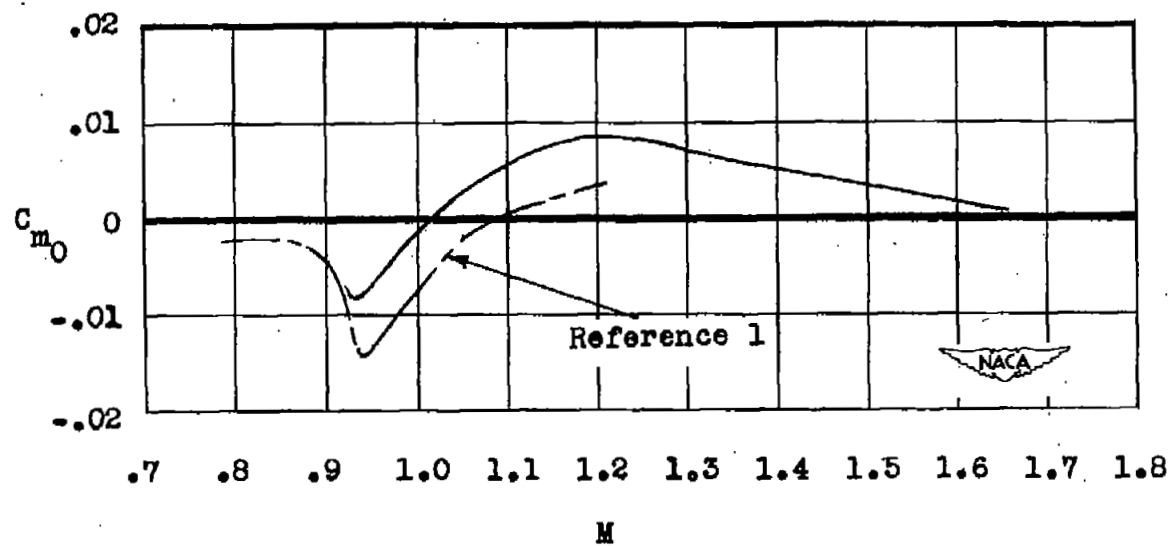


Figure 27.- Basic pitching-moment coefficient.

SECURITY INFORMATION



NASA Technical Library

3 1176 01436 4534

